# Multivariate Analysis of Beam Orbit at the KEKB Injector Linac

Aimin XIAO

July 21, 1999

**Abstract**

In this thesis, we will discuss multivariate analysis of beam orbit. The core of this work is Model-Independent Analysis (MIA) which was first introduced into accelerator physics by J. Irwin and his collaborators. This is a new method which can be used to do beam dynamic analysis in a real accelerator. It is based on the fact that the variables under study are correlated through the laws of dynamics. If we put them together and treat them as a whole then maybe we can obtain these correlations using some suitable algorithm. That is the starting point of multivariate analysis.

MIA is a method used in accelerator physics, which is based on the BPMs measurements to improve BPMs resolution and find out a realistic model for the real machine. It is a multivariate analysis method. Also, it does not rely on any particular machine model, and therefore it is called MIA.

At the beginning of this thesis, we briefly review what we can do with MIA. Trying to improve the accuracy of BPMs measurements is the first motivation for developing MIA. As we work more, we get more understanding of the method. Then we know how to use it to find out the machine model, wakefield effects, emittance dilution, etc. We are hopeful that we will be able to do more in the future with this method.

There are 4 main parts in this thesis. In the first part, we discuss the MIA method generally by introducing the Taylor expansion of the beam trajectory, removal of known time patterns, analysis by using SVD. In the last section of this part, we give a simple example to illustrate SVD analysis method.

In the second part, we review beam dynamics in linac. When the beam intensity goes up, wakefield effects become a serious part of the beam behavior. We write down the equation of motion in the presence of wakefields. From the equations, we can see that the transverse wakefields will cause an emittance dilution and the longitudinal wakefields will cause a correlated energy spread inside the bunch. We also review the emittance dilution due to

filamentation. When the beam is well matched to the machine, this will not be the main source of emittance dilution. To alleviate the emittance dilution and keep the correlated energy spread as small as possible at the end of linac, we need a technique called BNS damping and auto-phasing. All the theories introduced in this part will be used as the base of our simulation work in the next section.

In the third part, we used MIA method and our knowledge of beam dynamics in linac to do simulations. Through this work, we show how MIA works and what kind of results we can obtain from this method. We also investigate the limitations of this method through the simulations. The simulation work is based on the KEKB injector linac (Sec.A & Sec.B). First, we investigate the possible sources of beam orbit fluctuations. Then, we simulate these sources and examine their effects without wakefields. These results can be used to compare with the beam behavior when the beam current is quite low. Finally, we simulate the beam behavior with wakefields. From the results we can see the wakefield effects clearly, also the emittance dilution can be observed. At the end, we show that for different lattice structures and different beam orbits, the emittance dilution is not the same. These results can be a guide for alleviating the emittance dilution which must be carefully studied experimentally.

In the fourth part, we used the MIA method on our experimental data. The results do not only confirmed the MIA method and our simulation work, but also reveal a more realistic machine model. It opens new possibilities which is the most important thing: it tells us how to improve our machine in the future.

In the last part of this thesis, we conclude on what we have achieved and give a glimpse of what can be done as a next step.

# Contents


**1 Motivation** **8**

**2 Introduction to Model-Independent Analysis (MIA)** **11**

2.1 Taylor expansion of beam trajectory . . . . . 12

2.2 Removal of known time patterns . . . . . 14

2.3 Analysis using Singular Value Decomposition (SVD) . . . . . 16

2.4 A simple example to illustrate SVD . . . . . 18

**3 Introduction to beam dynamics in linac** **25**

3.1 Wakefields. . . . . 26

3.2 Equations of motion. . . . . 27

3.3 Emittance dilution . . . . . 30

3.3.1 Filamentation . . . . . 30

3.3.2 Transverse wakefield effects . . . . . 34

3.4 BNS damping . . . . . 35

**4 Simulation study** **37**

4.1 KEKB injector linac . . . . . 37

4.2 Contributions to beam orbit $\vec{b}_p$ . . . . . 40

4.3 Free betatron oscillations . . . . . 40

4.3.1 Pulse number $P$, BPMs resolution and bad BPM . . . 40

4.3.2 D.O.F analysis . . . . . 44

4.3.3 Machine model . . . . . 45

4.3.4 Energy jitter . . . . . 48

4.3.5 More general case . . . . . 48

4.4 Wakefields . . . . . 48

4.4.1 Short-range wake functions . . . . . 53

4.4.2 Misalignment effects . . . . . 56

4.4.3 Injection offset . . . . . 61

4.4.4 Orbit steering and Lattice re-matching . . . . . 64
4.4.5 BNS damping . . . . . 67

**5 Experimental results** **68**
5.1 Low beam current experiments . . . . . 78
5.2 High beam current experiments . . . . . 79

**6 Conclusions** **81**

**7 Future prospect** **82**

**8 Acknowledgment** **83**

**9 Appendix** **84**
9.1 Theoretical Analysis . . . . . 85
9.2 Experimental and Numerical Results . . . . . 89

# List of Figures


2-1 Eigenvectors and trajectories . . . . . 22
2-2 With BPM errors of $5\sigma_\xi$ and a vertical scale of $\pm 20$. . . . . 22
2-3 With BPM errors of one $\sigma_\xi$ and a vertical scale of $\pm 5$; . . . . 23
3-1 Two particles moving down the bore of a linac structure. . . . 26
3-2 Emittance dilution due to transvers wakefields . . . . . 27
3-3 Coordinate system along linac . . . . . 28
3-4 Chromatic filamentation of a mismatched beam. . . . . 31
3-5 Matched beam . . . . . 32
3-6 Dispersive filamentation of a coherent betatron oscillation. . . 33
4-1 Beta functions of the first 1.5 GeV Linac . . . . . 39
4-2 Singular value vs. pulse number $P$ . . . . . 41
4-3 Noise floor vs. BPMs number $M$ . . . . . 42
4-4 Variance between BPM reading and the real beam trajectories 43
4-5 Noise floor vs. BPMs resolutions . . . . . 44
4-6 Eigenvectors and bad BPM . . . . . 45
4-7 Injection jitter and kicker noise . . . . . 46
4-8 Calculated machine model without/with cutting the noise floor 47
4-9 Incoming beam jitter: $x_0$, $x_0'$, and $\Delta\delta = 2.5\%$ . . . . . 49
4-10 Incoming beam jitter: $x_0$, $x_0'$, and $\Delta\delta = 2.5\%$ . . . . . 50
4-11 Incoming beam jitter:$x_0$, $x_0'$,$\delta = 2.5\%$, magnet ripple and $\Delta\phi$ 51
4-12 Incoming beam jitter:$x_0$, $x_0'$,$\delta = 2.5\%$, magnet ripple and $\Delta\phi$ 52
4-13 Longitudinal wake function for KEKB injector linac . . . . . 54
4-14 Transverse wake function for KEKB injector linac . . . . . 54
4-15 Misalignment effects: High beam current . . . . . 57
4-16 Misalignment effects: High beam current-Machine model . . . 59
4-17 Misalignment effects: High beam current-Emittance dilution . 59
4-18 Misalignment effects: Low beam current ($\delta x_0 = 40\mu m$, $\delta x_0' = 40\mu rad$) . . . . . 60

4-19 Injection offset effects: High beam current . . . . . 62
4-20 Injection offset effects: Low beam current . . . . . 63
4-21 Orbit steering: emittance dilution and machine model . . . . . 64
4-22 Orbit steering: D.O.F analysis . . . . . 65
4-23 Re-matched lattice: Machine model and emittance dilution along the linac . . . . . 65
4-24 Re-matched lattice: D.O.F analysis . . . . . 65
4-25 Beta-function of re-mached lattice . . . . . 66
4-26 BNS damping: Machine model and emittance dilution along the linac . . . . . 67
4-27 BNS damping: D.O.F analysis . . . . . 67
5-1 Exp.: The average beam orbit . . . . . 69
5-2 Exp: Square root of the variance of beam orbits . . . . . 70
5-3 Exp: D.O.F analysis at low beam current . . . . . 71
5-4 Exp: D.O.F analysis at high beam current . . . . . 72
5-5 Exp: Machine model (ideal) and variance of beam orbits . . . 73
5-6 Exp: Eigenvalues and Eigenvectors . . . . . 74
5-7 Exp: Machine model and emittance growth rate along the linac 75
5-8 Exp: Eigenvalues and Eigenvectors . . . . . 76
5-9 Exp: Machine model and emittance growth rate along the linac . . . . . 77
9-1 Exp: Final Data at BPM # 20 expressed around the average. 90
9-2 Exp: Final Data at BPM # 20 expressed around the average. 91

# 1 Motivation

The KEKB-factory [6] is an asymmetric electron-positron collider at $8(e^-) \times 3.5(e^+)$ GeV. Its mission is to support high energy physics research programs on CP-violation and other topics in B-meson decays. Its luminosity goal is $10^{34} cm^{-2} s^{-1}$. In order to meet the requirement of full-energy injection of KEKB, the original PF (Photon Factory) injector linac was upgraded and used as the KEKB injector linac [7]. It can provide an 8.0GeV electron and a 3.5GeV positron single bunch beams for injection in the KEK B-factory. The designed beam intensities are 1.2nC/pulse electrons and 0.64nC/pulse positron. For positron production, an 3.7 GeV 10nC/pulse electron beam is produced and accelerated to the positron production target. How to deliver such an intensive single bunch beam successfully without serious degradation of beam quality is a big challenge. The emittance preservation and the stability of the beam orbit are two of the problems concerning us the most. They affect the injection efficiency seriously and therefore the performance of KEK B-factory.

The first motivation of our work is to try to improve the accuracy (or resolution) of BPM measurements. Once a BPM is constructed, its resolution is already fixed and it is hard to change it later. Also for technical and financial reasons, we cannot have them built to as high a resolution as we would wish. One possible way to achieve a greater resolution is to use the correlation between BPMs measurement. The measurements of BPMs are physically correlated with each other because they are part of a relatively stable dynamical system. If we use the BPMs to measure the beam orbit for the same pulse, and repeat the measurement for a big pulse number, then with the benefits of statistics and correlations between BPMs, the accuracy can be greatly improved. The improvement depends on the number of pulses and the number of BPMs, usually it can reach one order of magnitude or more.

The second motivation of our work is "noise" sources finding. In a real machine, we can always observe beam orbit fluctuations. Trying to make the beam orbit more stable, we need to know which changes of the variables cause the fluctuation and where it is located. To answer this question, we need to measure the beam orbit for many pulses and put all of our measurements together into a matrix. Then the problem is just equivalent to finding out the rank of a matrix. The rank of the whole set of BPMs reading matrix determines the degree of freedom of the beam motion. If we get the rank of a sub set of the matrix from the beginning of the beam line to an arbitrary location and trace the change of the rank as a function of location, then we can locate the variables.

Another motivation of our work is to find out a machine model (response function of variables) for the real machine. The lattice structure is designed by some computer code(s) (MAD [18], SAD [17], Transport [19], etc.), but the real machine could be different from our design one because of various errors and collective effects. Trying to get the real machine model becomes one of the most important things during operation. There are several methods to do this work, some of them use perturbation method and could not be running during machine operation, also sometimes the accuracy is not good enough. So, finding out an accurate method, which can obtain a machine model without disturbing the operation, is an important problem in accelerator physics. Multivariate analysis is such a method.

For modern linear accelerators, beam current is very high, and wakefield effects are much stronger than before. These effects depend strongly on the beam orbit, so we need to study them experimentally. They dominate beam behavior and are the main causes of beam emittance dilution. To reveal the effects experimentally and find out the source of emittance dilution is the aim of our work.

After we understand noise sources, the machine model and wakefield effects, we can find some way to solve the problems and make improvement in

our machine performance.

We make a brief introduction to Model-Independent Analysis method and single bunch beam dynamics in the linac at the beginning of this thesis. Then we describe how the method works and what the beam behavior in the KEKB injector linac probably is by simulation studies. In the simulations, we also introduce some methods (BNS damping, lattice re-matching and orbit steering) to alleviate emittance dilution which haven't been tried experimentally. Finally, we use this analysis method in the experiment, it works very well. Also, the experimental results agree well with our simulation study.

# 2 Introduction to Model-Independent Analysis (MIA)

Model-Independent Analysis (MIA) was first introduced into accelerator physics by J. Irwin and his collaborators [1, 2, 3, 4]. This method uses BPM-based observations to analyze beam dynamics in an accelerator. This analysis method does not rely on any particular machine model, and therefore it is called MIA.

There are two major methods which permit a model independent analysis.

1. The first method is based on the measurements of "time patterns" and the removal of their effects from the BPM readings.

2. The second method uses the "Singular Value Decomposition" of the BPM-reading matrix.

The two methods are complementary. In the first instance one takes advantage of known measured quantities which are responsible for the orbit fluctuations. For example if the initial positions and momenta, $(x_0, x_0')$, at the beam line entrance have fluctuations, then it is quite clear that the orbit will depend on these initial variables. For the case when these fluctuations can be accurately measured, Irwin proposed a method for removing the effects of these known quantities from the data. The second method is a noise reduction and a degree-of-freedom analysis using the singular value decomposition (SVD) of the BPM-reading matrix. In the above example, one can imagine that after the removal of the effects of $(x_0, x_0')$, there are still unknown sources affecting the beam trajectory. For example, if one dipole in the beam line has an unacceptable jitter, the trajectory beyond this dipole will be affected. Using SVD, one can try to locate the position along the beam line of various unknown sources.

Finally it is also remarkable that one can break the resolution limit set by individual BPMs and observe beam dynamics far more accurately. This

is true because the measurements from BPMs in an accelerator are highly correlated. The number (D) of degrees of freedom driving the beam centroid motion is much less than the number (M) of BPMs. If one puts the measurement results of all BPMs for a large number (P) of pulses into a matrix $B_{M\times P}$ (BPM-reading matrix), and performs an SVD on this matrix, then, because of the large statistical sampling and the correlation between BPMs of dynamical origin, we will indeed be able to resolve the dynamics to a level of precision higher than the resolution of the individual BPMs. Theoretically the contributions of each variable to the beam centroid motion can be identified within an accuracy of $\sigma\sqrt{D\ /\ PM}$ where $\sigma$ is the original BPM resolution.

MIA is a statistical analysis method. The BPM reading matrix can be collected non-invasively during normal machine operation. So, MIA is, to our knowledge, the first method that can get a model of the real machine without disturbing the machine itself. It is hoped that it will lead to a better understanding and control of the beam, and that it can be used both for linacs and storage rings.

In the rest of this section we describe the theoretical tools which are used in the rest of this thesis. Our goal is to make the thesis self-contained and also to provide a simple introduction to the methods since the literature is pretty sparse on this topic. We will not only describe the theory, but also provide some simple example that hopefully illuminate the entire method.

## 2.1 Taylor expansion of beam trajectory

The beam trajectory can be measured by a sequence of BPMs. It fluctuates from pulse to pulse. Let M denote the total number of BPMs along the beam line and P denote the total number of pulse measurements. The BPM reading matrix $B_{M\times P}$ can be constructed with the $p^{th}$ row vector

$\vec{b_p} \equiv$ ( $b_p^1$ $b_p^2$ $\cdots$ $b_p^M$ ). $\vec{b_p}$ represents the measured trajectory of p$^{th}$ pulse.

In a stable[1] case, all the pulses $\vec{b_p}$ are close to the average orbit $\langle \vec{b_p} \rangle$. The fluctuation of $\vec{b_p}$ depends on various physical variables such as the initial incoming conditions of the beam, the settings of magnets, and rf conditions. We Taylor expand the beam trajectory $\vec{b_p}$ over all variables and substract out the average term, we obtain:

$$\vec{b_p} - \langle \vec{b} \rangle = \sum_s \left( \Delta v_p^s - \langle \Delta v^s \rangle \right) \left. \frac{\partial b}{\partial v^s} \right|_{v \;\; s=\overline{v^s}} + \cdots + \vec{n}_p \tag{2.1}$$

where $\langle\rangle$ denotes an average over a large ensemble of pulses. $\Delta v = v - \overline{v}$, $\overline{v}$ indicates the nominal value of $v$. $v^s \in \{x_0, x'_0, \delta, \sigma_z, I, V_{rf}, \cdots\}$ , where $x_0, x'_0, \delta, \sigma_z, I, V_{rf}$ are respectively the initial beam position, initial angle, relative energy, bunch length, current, and rf voltage, given as examples of possible physical variables. $\vec{n}_p = \left\{ n_p^1, n_p^2, \cdots n_p^M, \right\}$ is the contribution from random BPM noise. In some cases, the higher order correlations are important: Irwin and Wang [39] introduce them as independent variables—thus Eq. (2.1) keeps the same form.

We define dimensionless temporal unit vectors $\vec{q^s}$ with their $p^{th}$ elements ($p \in \{1, 2, \cdots, P\}$ ) given by:

$$q_p^s \equiv \frac{\Delta v_p^s - \langle \Delta v^s \rangle}{\sqrt{P} (\Delta v^s)_{rms}} \tag{2.2}$$

and the corresponding spatial vectors $\vec{f_s}$

$$\vec{f_s} \equiv (\Delta v^s)_{rms} \frac{\partial \vec{b}}{\partial v^s} \tag{2.3}$$

have the dimension of length. Eq. (2.1) is then re-expressed as:

$$\hat{\vec{b}}_p \equiv \frac{\vec{b_p} - \langle \vec{b} \rangle}{\sqrt{P}} = \sum_s q_p^s \vec{f_s} + \hat{\vec{n}}_p \tag{2.4}$$

[1]The beam orbit is stable over time.

where $\widehat{\vec{n}}_p = \frac{\vec{n}_p}{\sqrt{P}}$

Eq. (2.4) tells us that a beam orbit is a linear combination of a limited number of "basic" orbits given by the $f_q$'s, while $f_q$'s is the response function of an accelerator to the variable $q$. Or in other words, the beam motion is a superposition of certain basic modes. We can rewrite Eq. (2.4) in a matrix form:

$$\widehat{B} = QF^T + N \tag{2.5}$$

where, $Q_{P\times d} = \left[\vec{q}^1, \cdots, \vec{q}^d\right]$ contains the information of variable's change with time; it is thus called the "time pattern." $F_{M\times d} = [\,\vec{f}_1, \cdots, \vec{f}_d\,]$ contains the information of variation of beam orbit at each BPM point, according to the variables change; it is called the "space pattern." $N_{P\times M}$ contains the information of BPM reading noise.

From now on, let $B = \widehat{B}$, $B$ denotes the BPM reading matrix.

## 2.2 Removal of known time patterns

Let us assume that a set of correlated time patterns is known to affect the BPM matrix and has been measured. For example, as we pointed out in the introduction, this set could be the initial position and momentum

$$(\,q^1, q^2\,) = (\,\frac{x_0 - \langle x_0\rangle}{\sqrt{P}\sigma_{x_0}}, \frac{x_0' - \langle x_0'\rangle}{\sqrt{P}\sigma_{x_0'}}\,)\,. \tag{2.6}$$

It would not be surprising if the correlation $\langle\, x_0 x_0' \,\rangle$ is non vanishing. For example if these fluctuations are caused by a few dipole jitters before the beam line, we would expect $\langle\, x_0 x_0' \,\rangle \neq 0$. Let us perform the following summation:

$$\sum_{p=1}^{P} q_p^1 \widehat{\vec{b}}_p = \sum_{p=1}^{P}\sum_s q_p^1 q_p^s \vec{f}_s + \; q_p^1 \widehat{\vec{n}}_p \tag{2.7}$$

If the number of pulses is large and the measurements are uncorrelated in time, then the sum over the number of pulses is equivalent to a statistical average. By assumption, we expect

$$\sum_{n=1}^{\infty} q_p^1 q_p^1 = \sum_{n=1}^{\infty} q_p^2 q_p^2 = 1$$
$$\sum_{n=1}^{\infty} q_p^1 q_p^2 = \frac{\left\langle \Delta x_0 \Delta x_0^{'} \right\rangle}{\sigma_{x_0} \sigma_{x_0'}} = \mathcal{C}_{12}. \tag{2.8}$$

All other correlations[2] must be close to zero for a large number of pulses. Consequently, we have a new expression relating the known time patterns to their space patterns:

$$\left(q^1, q^2\right)^T \widehat{B} = \begin{pmatrix} 1 & \mathcal{C}_{12} \\ \mathcal{C}_{12} & 1 \end{pmatrix} \begin{pmatrix} \vec{f_1} \\ \vec{f_2} \end{pmatrix} + O\left(\frac{1}{\sqrt{P}}\right). \tag{2.9}$$

Clearly Eq. (2.9) can be inverted and this leads to a solution for the space patterns:

$$\begin{pmatrix} \vec{f_1} \\ \vec{f_2} \end{pmatrix} = \begin{pmatrix} 1 & \mathcal{C}_{12} \\ \mathcal{C}_{12} & 1 \end{pmatrix}^{-1} \left(q^1, q^2\right)^T \widehat{B}. \tag{2.10}$$

The contribution from the known sources $(q^1, q^2)$ can then be removed from BPM matrix $\widehat{B}$. We are left with a "reduced" matrix $\widehat{B}'$ which hopefully does not contain influences from the set $(q^1, q^2)$:

$$\vec{\widehat{b}}_p' \equiv \sum_{s=3}^{D} q_p^s \vec{f_s} + \vec{\widehat{n}}_p' \tag{2.11}$$

[2]The correlations between $q^1$ $q^2$ and other variables may be not zero,

$$\left(q^1, q^2\right)^T \widehat{B} = \begin{pmatrix} 1 & C_{12} & C_{13} & \cdots \\ C_{12} & 1 & C_{23} & \cdots \end{pmatrix} \begin{pmatrix} \vec{f_1} \\ \vec{f_2} \\ \vec{f_3} \\ \vdots \end{pmatrix} + O\left(\frac{1}{\sqrt{P}}\right).$$

Normally, $C_{1m}$ and $C_{2m}$ $(m \geq 3)$ are quite small. Also the fluctuations of beam trajectories are dominated by $\vec{f_1}$ and $\vec{f_2}$ , $\vec{f_3}$ and so on are just under 1 order less than them. So, we can neglect it, this will only introduce some small errors ($\leq 10\%$ ) into our calculation.

## 2.3 Analysis using Singular Value Decomposition (SVD)

$$S_{mn} = \sum_{p=1}^{P} b_p^m b_p^n \ . \tag{2.12}$$

What is the significance of this object if any? In the absence of any dynamical knowledge, we can construct the following vector function in the BPM vector space:

$$\left\langle \vec{n} \cdot \vec{b} \right\rangle = \frac{1}{P} \sum_{p=1}^{P} \vec{n} \cdot \vec{b}_p \ . \tag{2.13}$$

We can then ask what unit vectors $\vec{n}$ maximize the quantity in Eq. (2.13), and immediately we see that it is simply the average value of the BPM matrix which, incidentally, we have already taken out. Therefore we can construct the variance of this quantity:

$$\left\langle \left(\vec{n} \cdot \vec{b}\right)^2 \right\rangle = \frac{1}{P} \sum_{p=1}^{P} \vec{n} \cdot \vec{b}_p \vec{n} \cdot \vec{b}_p \ = n^T S n. \tag{2.14}$$

Now, we can ask in the root mean square sense, what are the unit vectors $\vec{n}$ which maximize the variance of this vector function. Obviously they will be most relevant to the dynamics of the BPM. Since $S$ is a symmetric matrix we are guaranteed a sequence of real eigenvalues and eigenvectors. In addition, since it represents the evaluation of a positive variance, we can assume that the eigenvalues will be greater or equal to zero. Using this information, we can rewrite the BPM matrix as follows:

$$B = \begin{pmatrix} \hat{\vec{b}}_1 \\ \vdots \\ \hat{\vec{b}}_P \end{pmatrix} = \underbrace{\begin{pmatrix} \vec{u}_1 \\ \vdots \\ \vec{u}_P \end{pmatrix}}_{U} \underbrace{\begin{pmatrix} \Lambda_1 v_1^T \\ \vdots \\ \Lambda_m v_m^T \end{pmatrix}}_{\Lambda V^T}$$

$$\text{where } S\vec{v}_k = B^T B \vec{v}_k = \Lambda_k^2 \vec{v}_k. \tag{2.15}$$

Following Irwin, it is obviously tempting to compare Eqs. (2.15) and (2.5):

$$B = QF^T + N \Leftrightarrow \; B = U\Lambda V^T. \tag{2.16}$$

This is pure mathematics at this point. However there are a few things which will become apparent through examples. First of all, in the limit of $M$ (number of monitors) becoming infinite, the nonzero eigenvectors will be made of linear combinations of trajectories (or pieces of trajectories). This implies that indeed, as pointed out by Irwin, the resolution of the trajectories can become very good if the number of monitors is large enough. In practice one can know the trajectories to an accuracy greater than the individual BPM resolution. It is also important to have a large number of pulses for obvious statistical considerations.

We should point out that the eigenvectors are not necessarily the linearly independent trajectories even in the simplest of cases as we will shortly see. In other words they may not correspond to the terms removed by the time pattern analysis— they are complex linear combinations of those. However if the lattice ( under BPM examination) is sufficiently long and periodic, it does appear that the eigenvectors tend to be close to the original trajectories one would have obtained through a time pattern analysis (cosine and sine trajectories).

In conclusion, if noise can be isolated or reduced, we can see that it should be possible to relate both representations through experiments (real and numerical) and thus get a true understanding of the beam line and use it for control purposes. This demands a lot of effort and stable experiments which is not necessarily what was achieved in the present work.

In the next section we illustrate the rather abstract comments made here through a simple example.

## 2.4 A simple example to illustrate SVD

Consider the following simple trajectory for an ideal system in one dimension:

$$x(s) = x_0 \cos(s) + p_0 \sin(s) . \tag{2.17}$$

This could represent a solenoid channel for example. In any event, we are only trying to illustrate the method and thus it is not physically important at this stage. Let us imagine that the BPMs are placed at some locations $s_n$ along the beam line. Then in the absence of any fluctuation and with perfect monitors, we have

$$b^n = x_0 \cos(s_n) + p_0 \sin(s_n) . \tag{2.18}$$

Now let us first introduce random errors at the entrance in both position and momentum as well as some BPM noise:

$$b_p^n = (x_0 + \xi_p) \cos(s_n) + (p_0 + \zeta_p) \sin(s_n) + \nu_p^n . \tag{2.19}$$

Finally, to make things a bit more exciting, let us put a random kick in momentum at position $s_k$. The final expression for the BPM vector is:

$$\begin{aligned} b_p^n = &(x_0 + \xi_p) \cos(s_n) + (p_0 + \zeta_p) \sin(s_n) + \nu_p^n \\ &+ \pi_p \sin(s_n - s_k)\, \theta(s_n - s_k) . \end{aligned} \tag{2.20}$$

The variables $(\xi_p, \zeta_p, \pi_p, \nu_p^n)$ are random variables with zero averages. The function $\theta$ is the usual step function which is null for negative arguments and unity for positive values of its argument. We first examine analytically the "large sample" limit. We must substract the average:

$$\widehat{b}_p^n = \xi_p \cos(s_n) + \zeta_p \sin(s_n) + \nu_p^n + \pi_p \sin(s_n - s_k)\, \theta(s_n - s_k) . \tag{2.21}$$

We can write the BPM vector for the $p^{th}$ pulse as

$$\vec{\widehat{b}}_p = \frac{1}{\sqrt{P}} \left\{ \xi_p \vec{c} + \zeta_p \vec{s} + \vec{\nu}_p + \pi_p \vec{t} \right\} . \tag{2.22}$$

We clearly distinguish three trajectories that a time pattern analysis would find if we knew in advance the sources $(\xi_p, \zeta_p, \pi_p)$. These three trajectories are the regular cosine and sine trajectories spawning the entire beam line as well as a piece of the sine trajectory after the monitor $k$ where the dipole kick occurs. Let us construct the matrix $S$ for large $P$ and finite $M$:

$$\begin{aligned} S_{mn} &= \sigma_\xi^2 c_m c_n + \sigma_\zeta^2 s_m s_n + \sigma_\pi^2 t_m t_n + \Delta_{mn} \\ \text{where } \Delta_{mn} &= \langle \nu^m \nu^m \rangle \, \delta_{mn}. \end{aligned} \tag{2.23}$$

Here we have assumed uncorrelated position and momentum at the entrance just to make the example simpler. The matrix $S$ involves three vectors of "substance" and the matrix $\Delta$ for the noise. Let us act on the three vectors $\left(\vec{c}, \vec{s}, \vec{t}\right)$ with the matrix $S$:

$$\begin{aligned} S\vec{c} &= \sigma_\xi^2 c^2 \ \vec{c} + \sigma_\zeta^2 \vec{c} \cdot \vec{s} \ \vec{s} + \sigma_\pi^2 \vec{c} \cdot \vec{t} \ \vec{t} + \Delta\vec{c} \\ S\vec{s} &= \sigma_\xi^2 \vec{c} \cdot \vec{s} \ \vec{c} + \sigma_\zeta^2 s^2 \ \vec{s} + \sigma_\pi^2 \vec{s} \cdot \vec{t} \ \vec{t} \ + \Delta\vec{s} \\ S\vec{t} &= \sigma_\xi^2 \vec{c} \cdot \vec{t} \ \vec{c} + \sigma_\zeta^2 \vec{s} \cdot \vec{t} \ \vec{s} + \sigma_\pi^2 t^2 \ \vec{t} \ + \Delta\vec{t} \, . \end{aligned} \tag{2.24}$$

We must compare the noise matrix $\Delta$ with the rest of the terms in Eq. (2.24). The norms $\{c^2, s^2, t^2\}$ are of order $M$—the number of monitors. If we assume that the noise is the same in all monitors, then the matrix $\Delta$ is diagonal and is just:

$$\Delta = \sigma_\nu^2 \ I. \tag{2.25}$$

The relative importance of the noise part of Eq. (2.24) to the "trajectory" part is of order $1/M$. Thus we can hope to separate noise and true trajectories by a factor of $\sqrt{M}$. Obviously the noise is not exactly the same for all monitors as in Eq. (2.25). This means that a small noise component will mix and the main eigenvectors will not be exactly made of the trajectories. This is also true if the number of pulses is not large enough.

So again, under the equal noise level assumption, the matrix $\Delta$ is a multiple of the identity, and thus we can diagonalize the trajectory part only. Thus Eq. (2.24) reduces to

$$\begin{aligned} S\vec{c} &= \sigma_\xi^2 c^2\ \vec{c} + \sigma_\zeta^2 \vec{c}\cdot\vec{s}\ \vec{s} + \sigma_\pi^2 \vec{c}\cdot\vec{t}\ \vec{t} \\ S\vec{s} &= \sigma_\xi^2 \vec{c}\cdot\vec{s}\ \vec{c} + \sigma_\zeta^2 s^2\ \vec{s} + \sigma_\pi^2 \vec{s}\cdot\vec{t}\ \vec{t} \\ S\vec{t} &= \sigma_\xi^2 \vec{c}\cdot\vec{t}\ \vec{c} + \sigma_\zeta^2 \vec{s}\cdot\vec{t}\ \vec{s} + \sigma_\pi^2 t^2\ \vec{t}\,. \end{aligned} \tag{2.26}$$

Generally the eigenvectors of Eq. (2.26) will be complex linear combinations of $\left(\vec{c},\vec{s},\vec{t}\right)$, therefore let us specialize to simple cases. Consider the case

$$\begin{aligned} M &= 40 \\ s_n &= \frac{2\pi(n-1)}{M} = \frac{\pi(n-1)}{20}. \end{aligned} \tag{2.27}$$

In this case the beam line covers a region of $2\pi$ phase advance and the monitors are equally spaced. Furthermore the parasitic dipole kick happens right in the middle of the beam line. Let us make the position and momentum fluctuations equal and leave the dipole kick arbitrary:

$$\begin{aligned} \sigma^2 &= \sigma_\xi^2 = \sigma_\zeta^2 \\ \sigma_\pi^2 &= r^2\sigma^2. \end{aligned} \tag{2.28}$$

For this example, it is clear that

$$\begin{aligned} c^2 &= s^2 = \frac{M}{2} \\ t^2 &= \frac{s^2}{2} = \frac{M}{4} \\ \vec{t}\cdot\vec{s} &= -\frac{s^2}{2} = -\frac{M}{4} \\ \vec{c}\cdot\vec{s} &= \vec{c}\cdot\vec{t} = 0. \end{aligned} \tag{2.29}$$

The equation for the action of $S$ on the trajectories becomes

$$S\vec{c} = \Sigma\vec{c}$$

$$
\begin{aligned}
S\vec{s} &= \Sigma\vec{s} - \frac{r^2}{2}\Sigma\vec{t} \\
S\vec{t} &= -\frac{1}{2}\Sigma\vec{s} + \frac{r^2}{2}\Sigma\vec{t} \\
r^2 &= \frac{\sigma_\pi^2}{\sigma^2} \quad \text{and} \quad \Sigma = \frac{M\sigma^2}{2}.
\end{aligned} \tag{2.30}
$$

The three eigenvectors can be computed:

$$
\begin{aligned}
\vec{v}_1 &= \vec{s} + \left[1 - \frac{r^2}{2} - \frac{1}{2}\sqrt{4+r^4}\right]\vec{t} \\
\vec{v}_2 &= \vec{c} \\
\vec{v}_3 &= \vec{s} + \left[1 - \frac{r^2}{2} + \frac{1}{2}\sqrt{4+r^4}\right]\vec{t}.
\end{aligned} \tag{2.31}
$$

The eigenvalues are

$$
\begin{aligned}
\Lambda_1^2 &= \Sigma\left(\frac{2 + r^2 + \sqrt{4+r^4}}{4}\right) \\
\Lambda_2^2 &= \Sigma \\
\Lambda_3^2 &= \Sigma\left(\frac{2 + r^2 - \sqrt{4+r^4}}{4}\right).
\end{aligned} \tag{2.32}
$$

Because of the symmetries in the lattice, the solutions are particularly simple. One of them is indeed a trajectory while the two others are rather simple to understand. In fact, for very small values of $r$, one regains the pure sine solution as well as a new one $\vec{v}_3 = \vec{s} + 2\vec{t}$.

We can check these results numerically. Here is a plot of the BPM readings, the three eigenvectors and the two cosine and sine trajectories. The parameters for Figure 2-1 where chosen as follows:

$$
M = 40 \quad r = 1.5 \quad p = 10,000 \tag{2.33}
$$

The vertical light green lines show the BPM reading fluctuations: they extend from $-5$ to 5 units. The initial position and momentum fluctuations had a sigma of one unit. The BPM noise was zero. Therefore the agreement with

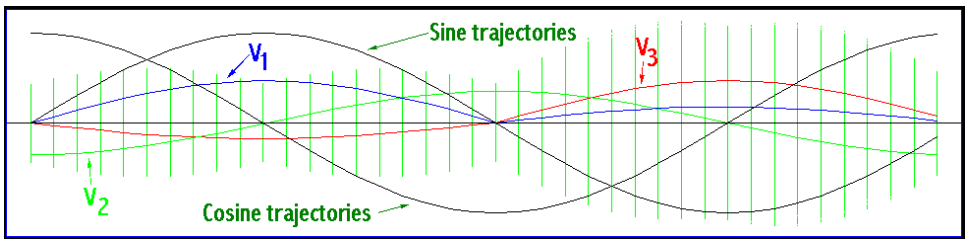


Figure 2-1: Eigenvectors and trajectories

the theory is near perfect. We do need still a large number of pulses in order to sample the statistical fluctuations correctly. For this particular example, analytical and numerical results agreed very well.

$$\begin{aligned} \text{Analytic} \quad & \Lambda_1 = 6.03 \quad \Lambda_2 = 4.4 \quad \Lambda_3 = 2.4 \\ \text{Numerical} \quad & \Lambda_1 = 6.09 \quad \Lambda_2 = 4.45 \quad \Lambda_3 = 2.47 \quad . \end{aligned} \tag{2.34}$$

At this point it is interesting to introduce BPM errors. In Figure 2-2, we

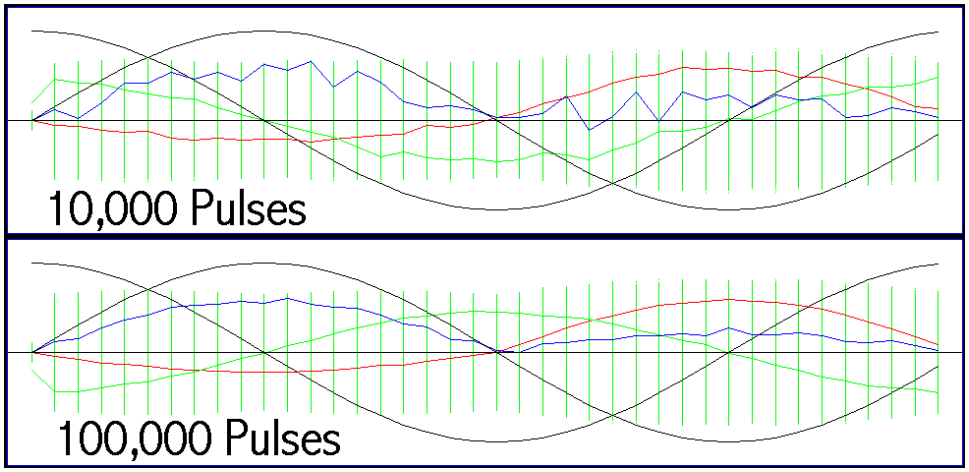


Figure 2-2: With BPM errors of $5\sigma_\xi$ and a vertical scale of $\pm 20$.

introduced BPM errors which are 5 times larger than the effect being measured. We are nevertheless seeing the 3 eigenvectors even with only $10,000$

pulses. Again we emphasize that all the monitors have equal resolutions.

On the other hand, if fluctuations in the monitor resolutions are introduced, because the noise matrix $\Delta$ of Eq. (2.24) does not commute with the trajectories, the true trajectories become harder to identify. This can be checked with this toy model and it shows up very clearly. In Figure 2-3 the error of the monitor is modulated by the same random variable. So

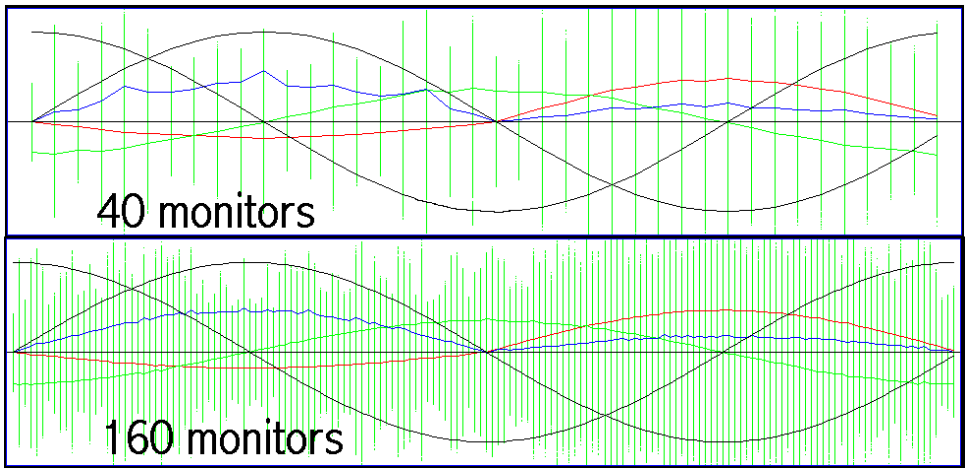


Figure 2-3: With BPM errors of one $\sigma_\xi$ and a vertical scale of $\pm 5$;

some monitors are much better and some are potentially $\sqrt{3}$ worse than the average monitor. (This factor comes from the fact that we use a uniform distribution. This distribution must produce numbers between $-\sqrt{3}$ and $\sqrt{3}$ in order to have a unit variance and zero average.) One can see how an increase in the number of monitors improves the situation. In a realistic situation, we do not have this option, but we can use a statistical technique to "cut the noise floor." This will be discussed in the section on the simulation of KEKB.

In this section we have not shown "time pattern" examples since it is quite clear that it takes each trajectories in correlated groups. We have seen that the SVD produces, in the limit of many pulses and many BPMs, the

main eigenvectors that are linear combinations of the fundamental trajectories. This example was shown only for illustrative purposes and does not have a real physical relevance to the KEKB beam line studied in this work. Nevertheless such things are always useful if one wants to understand obscure features of the SVD method.

In the following sections of this thesis, we discuss the application of these methods on the KEKB example.

# 3 Introduction to beam dynamics in linac

Beam dynamics issues in a linear accelerator have been discussed in many works [20, 9, 11, 13, 14, 15, 12, 21]. Papers [11, 13] give out a good survey on this topic. Among all of these issues, the beam orbit variation and the emittance dilution are two of the most important problems in linac. They set the main limitation of machine performance. Normally, a beam orbit variation is always accompanied with a beam emittance dilution, this is because of the existence of wakefields. In addition single particle effects (beta mismatch, dispersion effects, RF deflections, etc.) also can cause a significant emittance dilution. A list of sources causing effective emittance dilution in linacs is given in Table I.

Table I. List of sources causing emittance dilution.

1. Beta mismatch.
2. Dispersion effects.
3. RF deflections.
4. Trajectory jitters.
5. Transverse wakefields.

In this chapter, we will discuss effects that can enlarge the beam emittance during acceleration. A brief description of wakefield is reviewed at first. Then we write down the equations of motion in a linac. After that, we discuss emittance dilution due to dispersion effects and transverse wakefields. At the end, one of the most effective techniques for alleviating emittance dilution, which was proposed by Balakin-Novokhatsky-Smirnov (BNS damping) [20], is included in this work.

## 3.1 Wakefields.

When a charged particle travels down a linac, it interacts with the accelerator structure and creates a wakefield. This field acts on the particles following it. It changes the energy (longitudinal wake) and the displacement (transverse wake) of the following particles. Figure 3-1 shows two particles moving down the bore of a linac structure. The longitudinal wake does not depend on either

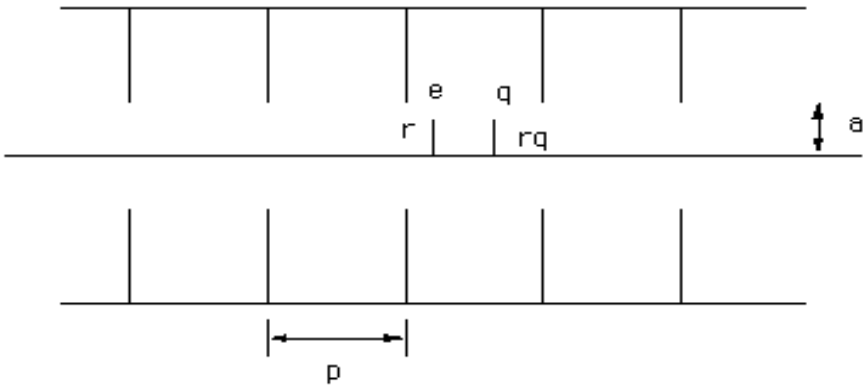


Figure 3-1: Two particles moving down the bore of a linac structure.

the radius or the azimuth. The average field $E_Z$ on the trailing particle is given by:

$$E_Z p \;=\; -\, q w_L(\tau) \tag{3.1}$$

where $w_L$ is the longitudinal wake potential of a unit charge. It depends on the accelerator structure and can be calculated by several computer codes (TBCI [22], ABCI [23], etc.). $\tau \;=\; (Z_{head} - Z_{tail}) \;/\; c$ is the time lag between these two particles. $p$ is the length of a period of the accelerator structure, $E_Z$p is the energy loss of a particle in the length of one period of the linac accelerator structure due to wakefields.

The transverse wakefield that concerns us most is called the dipole wake. It is independent of the radial position of the following charge but depends

linearly on the radial position of the source particle. The average field $\vec{E}_T$ on the trailing particle is given by:

$$\vec{E}_T p \;=\; q w_T(\tau)\,\frac{r_q}{a}\left(\vec{r}\cos\,(\Phi)\;-\;\vec{\Phi}\sin\,(\Phi)\right) \tag{3.2}$$

where $w_T$ is the transverse dipole wake potential, $r_q$ is the displacement of the leading particle from the linac axis, $a$ is the iris aperture, $\Phi$ is the azimuth, and $\vec{r}$ and $\vec{\Phi}$ are unit vectors.

The transverse wakefields occurs when the beam is not travelling along the axis of accelerator structure. It gives a transverse kick to the tail particles of the bunch and whips it to large amplitudes of oscillation. This results in an increase of the effective emittance. See Figure 3-2.

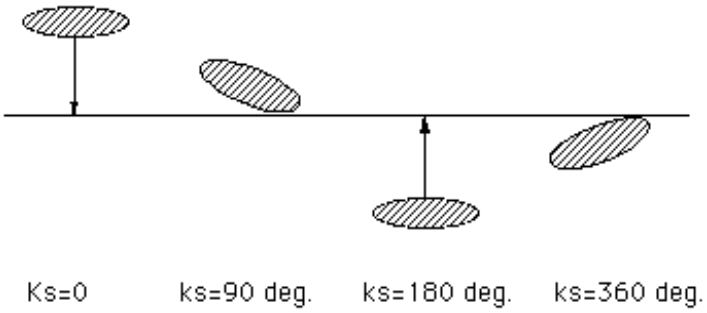


Figure 3-2: Emittance dilution due to transvers wakefields

## 3.2 Equations of motion.

A particle which travels down a linac will feel several kinds of forces.

1. Transverse focusing forces (from the external focusing system).
2. RF acceleration force (from the acceleration system).
3. wakefields (from the leading particles).

In the previous section, we already gave out a primary description of wake fields. Now we will write down the equations of motion including all of the effects indicated above.

In a high energy linear accelerator, the longitudinal motion is effectively independent of the transverse motion, also the longitudinal position is essentially fixed. So we can parameterize a particle's transverse motion with its longitudinal coordinates $(z, s)$. $s$ and $z$ are the longitudinal position in the accelerator and in the bunch. The coordinate system is illustrated in Figure 3-3. The dominant effects to the beam transverse motion in a linear accelera-

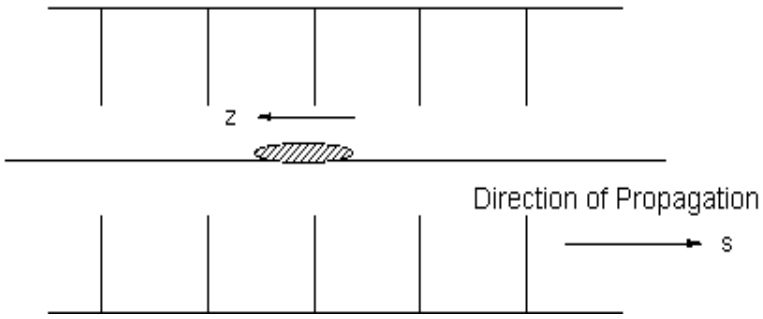


Figure 3-3: Coordinate system along linac

tor are the magnetic focusing field and the transvers dipole wakefield. Thus, the transverse equation of motion can be written as [37]:

$$\frac{d}{ds}\left(\gamma\left(s\right)\frac{d}{ds}x\left(z,s\right)\right)+\left(\frac{2\pi}{\lambda\left(s\right)}\right)^{2}\gamma\left(s\right)x\left(z,s\right) = r_{0}\int_{-\infty}^{z}dz'\rho\left(z'\right)w_{T}\left(z-z'\right)x\left(z',s\right) \tag{3.3}$$

where $\gamma(s)$ is the energy of the beam at position $s$ in unit of $mc^2$, $m$ is the rest mass of the electron. $\lambda(s)$ is the instantaneous wave length of betatron focusing at position $s$. $r_0 = e^2 / mc^2$ is the classical radius of the electron. $\rho(z)$ is the line density of the particles in the bunch ($\int \rho dz$ is normalized to the total number of particles in the bunch, N). $ew_t x$ is the transverse

wakefield produced by a point charge ($z'$) displaced from the axis by $x$ at a distance $z - z'$ behind the point charge.

Now, we will talk about the longitudinal equations of motion. As we mentioned before, the longitudinal position $z$ is fixed, only the relative energy deviation $\delta$ is changed during acceleration. The energy spread consists of two components: an uncorrelated energy spread which comes from the finite longitudinal emittance and an energy spread which is correlated with $z$. The correlated energy spread is due to the initial status, the longitudinal fields, and the acceleration RF voltage. We will calculate the correlated energy spread.

The energy gain of a particle in the bunch depends on its longitudinal position $z$ with respect to bunch center:

$$\Delta\varepsilon_{rf}(z,s) \;=\; eE_{rf}s\;\cos\left(\Phi_{rf} \;+\; \frac{2\pi}{\lambda_{rf}}(z-z_0)\right) \tag{3.4}$$

where $E_{rf}$ is the accelerating gradient, $\phi_{rf}$ is the phase of the bunch center with respect to the rf wave crest, $\lambda_{rf}$ is the wavelength of the acceleration mode and $s$ is the longitudinal position of the particle along the linac.

The energy loss of a particle in the bunch due to wakefields depends on its longitudinal position within the bunch, and is the convolution of the point charge longitudinal wake potential $w_z$ and the charge distribution $\rho(z)$ of the bunch.

$$\Delta\varepsilon_w(z,s) \;=\; e\int_{-\infty}^{z}\rho(z')\,w_z(z\;-\;z',s)\,dz' \tag{3.5}$$

For a uniform accelerating section, the longitudinal wake potential depends linearly on the bunch position along the linac. Then, the energy loss of a particle within the bunch along the linac may be written as:

$$\Delta\varepsilon_w(z,s) \;=\; eN\frac{s}{L_s}W_z(z) \tag{3.6}$$

where $N$ is the total charge of the bunch. $W_z$ is the longitudinal wake potential of the bunch after the bunch passes one accelerating section, $L_s$ is the length of accelerating section.

The net energy gain of a particle within the bunch will be the superposition of the rf accelerating potential and longitudinal wake potential.

## 3.3 Emittance dilution

In this section, we will discuss 2 main forms of emittance dilution that can increase the effective (design) beam emittance: filamentation due to the uncorrelated energy spread, and transverse wakefields. The proper correlated energy deviation is used to (partially) cancel the effect of the transverse dipole wakefield. This is called BNS damping, and will be discussed in the next section.

### 3.3.1 Filamentation

Energy spread in a beam will cause a frequency spread of betatron oscillation, and produce filamentation. The energy dependent filamentation can be divided into two categories: dispersive and chromatic filamentation. Dispersive filamentation occurs when the beam performs a coherent oscillation, and is referring to the filamentation of an oscillation. Chromatic filamentation occurs when the beam is not matched to the focusing structure of the machine, and is referring to the filamentation of the beam ellipse.

Since the particles' longitudinal position $z$ is fixed in a linac, we can divide the beam longitudinally into slices of constant $z$, each slice has a specified correlated energy deviation which will be discussed in next section. In this section we only care about the beam motion in one of the slices. We can subdivide it into slices of constant $\delta_{un}$, the uncorrelated energy deviation.

- Chromatic filamentation

Chromatic filamentation occurs when the beam phase ellipse is not matched to the machine ellipse. This can be illustrated in Figure 3-4. The lower

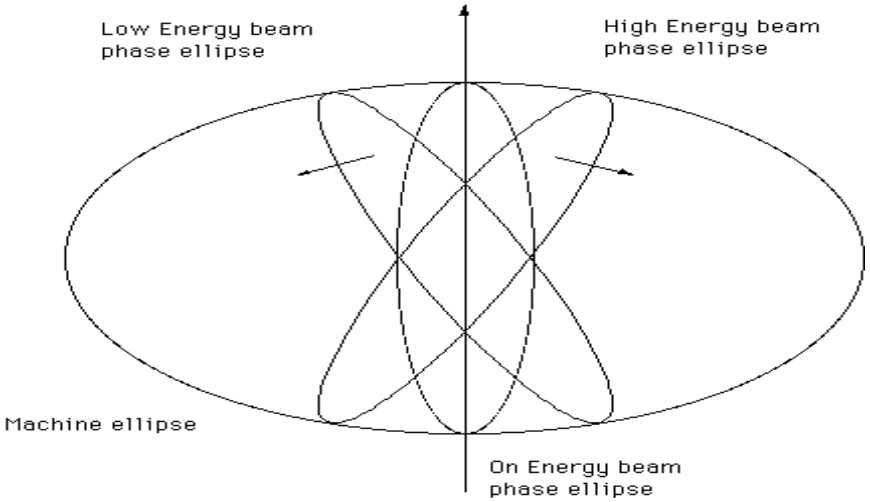


Figure 3-4: Chromatic filamentation of a mismatched beam.

energy particles will feel more stronger focusing force than the higher energy particles, and the phase ellipse of the lower energy particles rotates within the machine ellipse more quickly than that of the higher energy particles. In this case, the beam will filament to fill the machine ellipse, the design emittance is diluted. If the beam phase ellipse is matched to the machine ellipse, though the particles with different energy have different oscillation frequencies, they rotates within the machine ellipse (= beam ellipse) as the illustration in Figure 3-5. The design emittance is preserved.

The emittance dilution due to filamentation of a beta mismatch can be written as [27]:

$$\begin{aligned} \frac{\Delta\varepsilon}{\varepsilon} &= \frac{1}{2}\left(\frac{\beta}{\beta^*} + \frac{\beta^*}{\beta}\right) \\ &+ \frac{1}{2}\left(\alpha^*\sqrt{\frac{\beta}{\beta^*}} - \alpha\sqrt{\frac{\beta^*}{\beta}}\right)^2 - 1 \end{aligned} \tag{3.7}$$

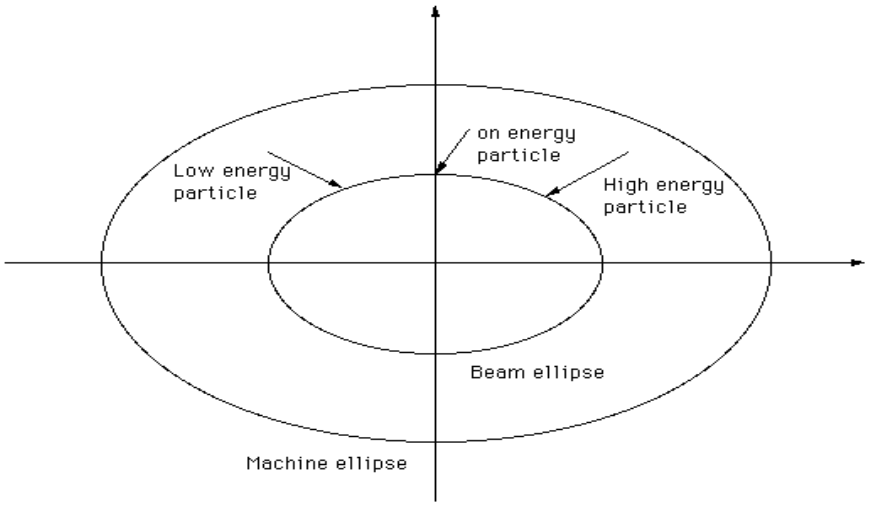


Figure 3-5: Matched beam

where $\alpha$ and $\beta$ are the machine parameters and $\alpha^*$ and $\beta^*$ are the beam parameters. Suppose, we match the beam at a symmetry point: $\alpha = 0$. Eq. (3.7) gives out the tolerances of lattice parameters matching.
Normally, the chromatic filamentation is not complete in a linac. The degree of filamentation can be estimated from the chromatic phase advance $\delta\nu_{rms}$ for particles with the rms energy deviation $\delta_{rms}$:

$$\delta\nu_{rms} = \frac{1}{4\pi}\int_0^L \delta_{rms} K_1 \beta ds \tag{3.8}$$

where $K_1$ is the normalized quadrupole strength.
A dispersion mismatch will also cause emittance dilution. Assuming full filamentation, the emittance dilution due to residual dispersion at the beginning of linac is [28]:

$$\Delta\epsilon = \frac{H_x \sigma_\epsilon^2}{2} \tag{3.9}$$

where $H_x \equiv \gamma_x \eta_x^2 + 2\,\alpha_x \eta_x \eta'_x + \beta_x \eta'^2_x$

- Dispersive filamentation

Dispersive filamentation occurs when the beam performs a coherent oscillation. This is illustrate in Figure 3-6. The frequency of the centroid beam oscillation with lower energy is higher than that with higher energy. As the beam filaments, it will fill an annular region in the machine ellipse, and the amplitude of the initial coherent oscillation decays.

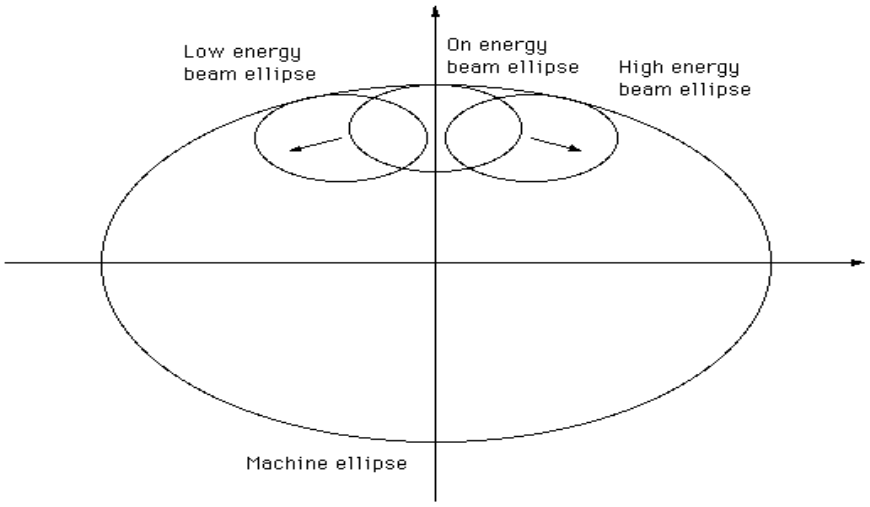


Figure 3-6: Dispersive filamentation of a coherent betatron oscillation.

There are two types of coherent oscillation: injection offset and a trajectory corrected to zero the BPMs. The full emittance filamentation due to injection offset can be written as:

$$\Delta\epsilon \;=\; \frac{1}{2}\left(\gamma_x\; x_0^2 \;+\; 2\;\alpha_x\; x_0\; x'_0 \;+\;\; \beta_x\; x'^2_0\right) \tag{3.10}$$

where $x_0$ and $x'_0$ are the initial amplitudes of the betatron oscillation.

Compare to the wakefield effects, the emittance dilution due to filamentation is quite small and can be easily corrected at the beginning of operation. For intense beams, the most important emittance dilution is coming from the transverse wakefields. So in the following discussion, we suppose that

the beam has already been matched to the machine, and concentrate our efforts to the wakefields effects.

### 3.3.2 Transverse wakefield effects

As a bunch travels down the bore of accelerating structures, wakefields are excited and act back on the bunch itself. The longitudinal wakefields introduce an energy spread along the bunch, the transverse wakefields tend to deflect the tail particles further away from the axis, leading to emittance dilution.

Normally, the dipole transverse wakefield is the dominant contributor to emittance dilution. The equation of motion for $x(z,s)$ is given by Eq. (3.11):

$$\frac{d}{ds}\left(\gamma(s)\frac{d}{ds}x(z,s)\right) + k(z,s)^2\gamma(s)\,x(z,s) = Nr_0\int_{-\infty}^{z} dz'\rho(z')\,w_T(z-z')\,x(z',s) \quad (3.11)$$

Here, $\int \rho dz = 1$. Now, we will use the two particles model which is the simplest one but still contains the essential of the physics. In this model, a Gaussian bunched beam is represented by two macro-particles, each particle has the charge of $\frac{N}{2}e$ (N is the total number of particles in the bunch), the two macro-particles are separated by a longitudinal distance $\Delta z = 2\sigma_z$. The head particle $x_1(0,s)$ does not feel any wakefields and goes down the linac with free betatron oscillations. The tail particle $x_2(z,s)$ oscillates according to the following equation:

$$x_2'' + \frac{\gamma'}{\gamma}x_2' + k^2 x_2 = \frac{Nr_0}{2}w_T(z,s)\frac{x_1(0,s)}{\gamma(s)} \quad (3.12)$$

The solution of this inhomogeneous equation may be written in terms of the transport matrix $M(s_0,s)$ and for the relative displacement of the tail

particle with respect to the head one, we get:

$$\Delta x\left(s\right) \;=\; \frac{r_0 N}{2} w_T\left(z\right) \int_0^s M_{12}\left(s',s\right) \frac{x_1\left(s'\right)}{\gamma\left(s'\right)} ds' \tag{3.13}$$

with

$$M_{12}\left(s',s\right) \;=\; \sqrt{\beta\left(s\right)\beta\left(s'\right)} \sqrt{\frac{\gamma\left(s'\right)}{\gamma\left(s\right)}} \sin\;\left(\Phi\left(s\right) \;-\Phi\left(s'\right)\right) \tag{3.14}$$

$$x_1\left(s\right) \;=\; x_0 \sqrt{\frac{\beta\left(s\right)}{\beta_0}} \sqrt{\frac{\gamma_0}{\gamma}} \cos\;\left(\Phi\left(s\right) \;-\theta\right) \tag{3.15}$$

$x_0$ and $\theta$ is the initial beam position and angle.

An emittance dilution is defined as the squared of the tail particle's displacement averaged over all phases. In order to estimate it, we use the well-known lattice scaling law [29]: beta function grows with the square root of the energy along the linac. Suppose there is no correlated energy spread along the bunch $\Delta\gamma = 0$:

$$\Delta\epsilon\left(s\right) \;=\; \frac{\langle \Delta x^2 \rangle}{\beta\left(s\right)} \;=\; \frac{x_0^2}{\beta_0} \left(\frac{N r_0 w_T\left(z\right)}{4}\right)^2 \frac{\gamma_0}{2\gamma_f} \left(\frac{\overline{\beta_f}}{G}\right)^2 \tag{3.16}$$

where $G$ is the acceleration gradient in $\Delta\gamma$ per meter and $\bar{\beta}$ is the average beta function in a FODO cell.
$\Delta\epsilon(s)$ is proportional to $x_0^2$ and $N^2$.

## 3.4 BNS damping

One of the most effective techniques for alleviating emittance dilution due to transverse wakefields was proposed by Balakin, Novokhatsky and Smirmov (BNS damping) [20]. Theoretical studies and some applications of BNS damping has been performed in a number of papers [24, 25, 26]. The essential point of BNS damping is to compensate the transverse wakefield effects by introducing a varying focusing strength along the bunch.

Let us consider the two particles model again. Particle 2 has an energy of $\gamma_1 + \Delta\gamma$. We use a linear function $w = W_1 z$ to express the transverse wakefield (It is almost the real case when the bunch length is quite small). Then the equation of motion for particle 1 and 2 can be written as:

$$\begin{aligned} x_1'' + k_0^2 x_1 &= 0 \\ x_2'' + (k_0 + \Delta k(z))^2 x_2 &= \frac{Ne^2}{2E} w(2\sigma_z) x_1, \end{aligned} \tag{3.17}$$

where $k_0$ is the average focussing strength along the beam line. Using Eq. (3.17), to keep the motion of particle 2 identical to that of particle 1, the following equation must be approximately true along the beam line:

$$2k_0 \Delta k(z) x_2 = \frac{Ne^2}{2E} w(2\sigma_z) x_1.$$

Here $\Delta k(z)$ is created by changing the energy distribution along the bunch. It is easy to understand physically. Because the transverse wakefield always tends to deflect the tail particle off axis, if the tail particle has a smaller energy ($\Delta\gamma < 0$), it will get extra focusing from the quadrupoles, then the effects of wakefield will have been compensated.

BNS damping requires a correlated energy spread along the bunch, also the longitudinal wakefields will cause a correlated energy spread along the bunch. In order to get the benefits of BNS damping and to keep the energy spread as small as possible at the end of the linac at the same time, we need to scale the linac more carefully and adjust the rf accelerating phase. The criterion, for satisfying both BNS damping and also beam energy spread, is called auto-phasing.

# 4 Simulation study

With the knowledge of the previous two sections, we can study the beam behavior by simulations. The simulation work is done under various situations, which can happen in a practical machine.

First of all, we investigate the effect of each possible variable (such as: injection jitter, magnet noise, rf noise, beam current, bunch length, misalignments, etc.) individually on the beam behavior, thus we get some very simple physical images which tell us how the beam is sensitive to various variables.

Then we mix some variables together to make our simulation work more complicated and more realistic, we get some complicated images. Some of the results can be used to compare with the experiments. This work leads us to a clear understanding of the theory and the experiment.

The simulation work is based on the KEKB injection linac [7](Sec.A, Sec.B). The program SAD [17] is used to simulate various conditions and generate the BPMs reading matrix. Mathematica [16] is the tool for data analysis. Our work is concentrated on the effects that cause the centroid beam orbit fluctuation.

## 4.1 KEKB injector linac

The KEKB-factory [6] is an asymmetric electron-positron collider at $8(e^-) \times 3.5(e^+)$ GeV. Its mission is to support high energy physics research programs on CP-violation and other topics in B-meson decays. Its luminosity goal is $10^{34} cm^{-2} s^{-1}$. The main parameters of KEKB are listed in Table 1.

Table 1: Main parameters of KEKB-Factory

| Ring | | LER($e^+$) | HER ($e^-$) | |
|---|---|---|---|---|
| Energy | E | 3.5 | 8.0 | GeV |
| Circumference | C | 3016.26 | | m |
| Luminosity | L | $1 \times 10^{34}$ | | $cm^{-2}s^{-1}$ |
| Beam current | I | 2.6 | 1.1 | A |

In order to meet the requirement of full-energy injection of KEKB, the original PF (Photon Factory) injector linac was upgraded to KEKB injector linac. It contains 3 parts, a new additional linac which can accelerate the electron to 1.5GeV, the original one which was upgraded to 6.5GeV, and they are connected by a 180 degree arc. A 1.2nC/pulse single bunched electron beam and a 0.64nC/pulse single bunched positron beam can be accelerated to 8.0 GeV and 3.5 GeV respectively at the end of the linac. For positron production, an 3.7 GeV 10nC/pulse electron beam is produced and accelerated to the positron production target. The main parameters of KEKB injector linac are listed in Table 2.

Table 2: Main parameters of KEKB Injector Linac

| | | $e^-$ | $e^+$ | |
|---|---|---|---|---|
| Energy | E | 8.0 | 3.5 | GeV |
| Bunch width | $\sigma_z$ | | 5 | ps |
| Particles/pulse | | $8 \times 10^9$(1.28) | $4 \times 10^9$(0.64) | (nC) |
| | | | $6.25 \times 10^{10}$(10 $e^-$) | |
| Energy width | $\delta$ | 0.125% | 0.25% | |

Depending on the BPM reading system (measure beam position for the same pulse), only the new 1.5 GeV linac (Sec.A, Sec. B) is included into our simulation work. The placement of quadrupoles and the beta functions are illustrated in Figure 4-1. The first 13 sets of quadrupoles (Sec.A) are used to match the beam to the lattice down stream. The other sets (Sec.B) of

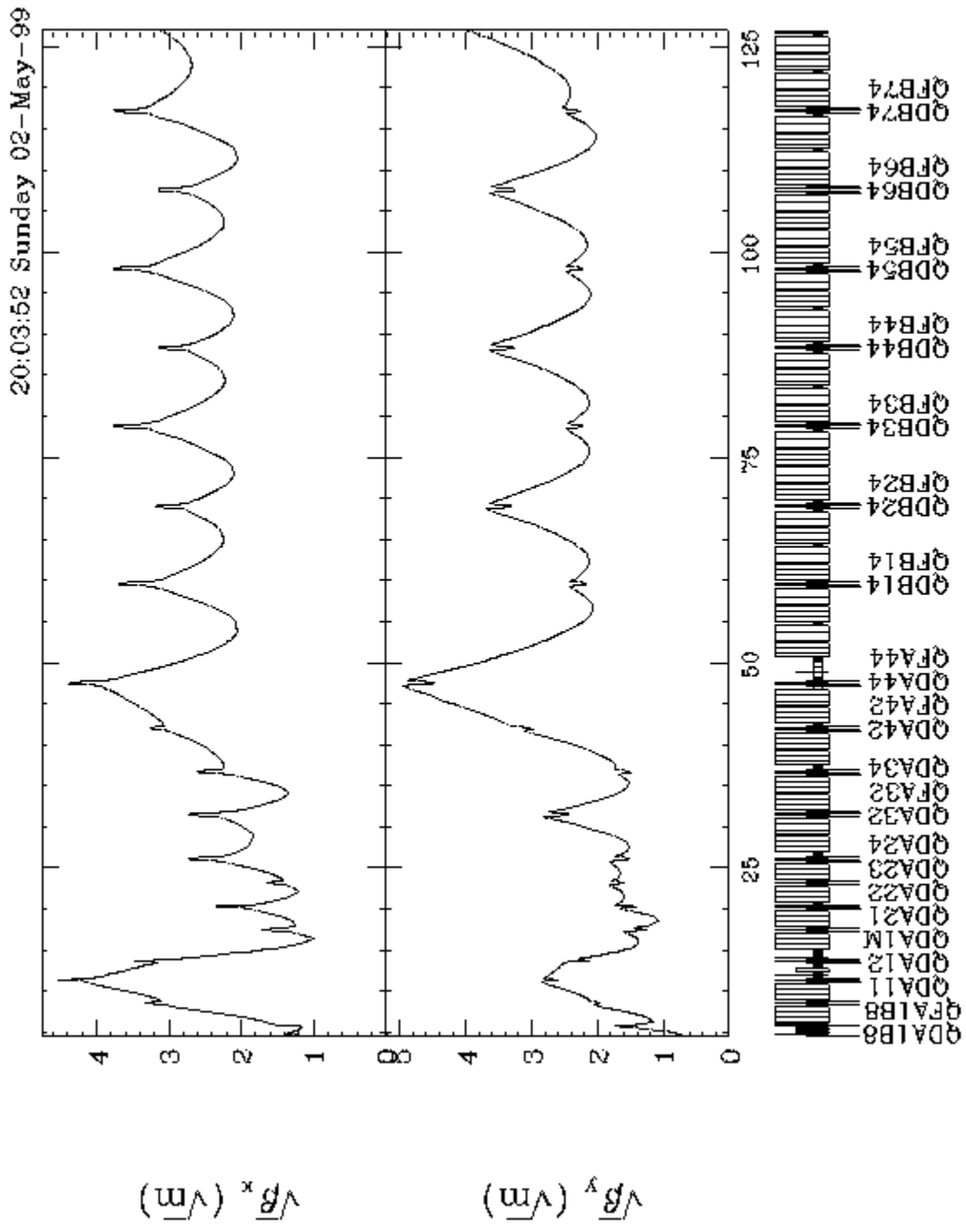


Figure 4-1: Beta functions of the first 1.5 GeV Linac

quadrupoles have their focusing strength set to achieve almost 90 degree betatron phase advance per cell. Just in front of each set of quadrupoles we installed a BPM to measure the beam position. The total numbers of BPMs (M) is 21.

## 4.2 Contributions to beam orbit $\vec{b}_p$

As we mentioned in Sect. 2, MIA is a new method to do beam dynamic analysis in a real machine. It relies on BPMs reading matrix B. While B is influenced by many kind of sources which are briefly listed below [3, 10]:

1. Constant $\vec{b}_0$: it comes from the stable centroid beam orbit and BPM offsets.

2. Injector conditions: include position ($\Delta$x, $\Delta$y), angle ($\Delta x'$, $\Delta y'$), energy ($\Delta\delta$), phase($\Delta\Phi_{inj}$), current ($\Delta$I), bunch length ($\Delta\sigma_z$), etc.

3. Products of injector conditions: $\Delta$x$\Delta$I, $\Delta$x$\Delta\Phi_{inj}$, $\Delta$x$\Delta\delta$, etc.

4. Beam line components change: accelerating voltage ($\Delta V_{rf}$), accelerating phase ($\Delta\Phi_{rf}$), magnet field ripple ($\Delta V_{corr}$, $\Delta V_{Quad}$), etc.

5. Ground motion, magnet vibration, accelerator-structure vibration, etc.

6. BPM noise, digitization, etc.

## 4.3 Free betatron oscillations

From now on, we start to simulate the beam without wakefields. The BPMs resolutions used here are $0.1mm$ with a $\sigma = 0.02mm$ distribution.

### 4.3.1 Pulse number $P$, BPMs resolution and bad BPM

- Pulse number $P$ and BPMs number $M$.

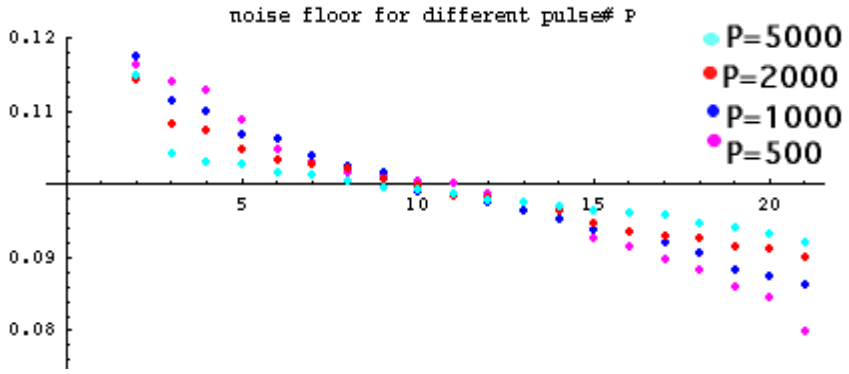


Figure 4-2: Singular value vs. pulse number $P$

The pulse number $P$, to be used to do the analysis, has a big effect on the accuracy of our simulation work and also experimental results. This effect is shown in Figure 4-2. In this simulation, we suppose that the beam orbit fluctuation comes from a position ($\sigma_x = 0.4mm$) and an angle ($\sigma'_x = 0.4mrad$) jitter at the beginning of the linac. Under these assumptions, we generate a BPM reading matrix B with 5000 pulses times 21 BPMs. Carrying out SVD on the B matrix, we get 3 new matrices: $U$, $\Lambda$, and $V$. First, let us consider the singular value matrix $\Lambda$. We plot the singular value $\lambda_m$ vs. $M$, and we call this "S.V. plot." Figure 4-2 shows the S.V. plot changes vs. pulse number $P$. In this plot, we can see that for $P = 500$ and $P = 1000$ the second singular value is mixed with the BPMs noise; but for $P = 2000$ and $P = 5000$, it begins to rise above the "noise floor." With the exception of the two largest singular values, which indicate the number of sources causing beam orbit fluctuation, other singular values e just form a "noise floor." When the pulse number $P$ increases, this floor becomes flatter. It is obvious that if $P$ is infinite and if all BPMs have the same resolution, then this floor becomes a horizontal line, and the value of this line is just the same as the BPMs resolution. From statistical principles, the accuracy can be improved by $\sqrt{P}$. In the following simulations, we choose $P = 5000$. Furthermore,

we can take out SVD for different BPMs number $M$. For similar reasons as with pulse number $P$, when $M$ increases, the noise floor decreases. Figure 4-3 gives out the noise floor change with increasing BPM number. The noise

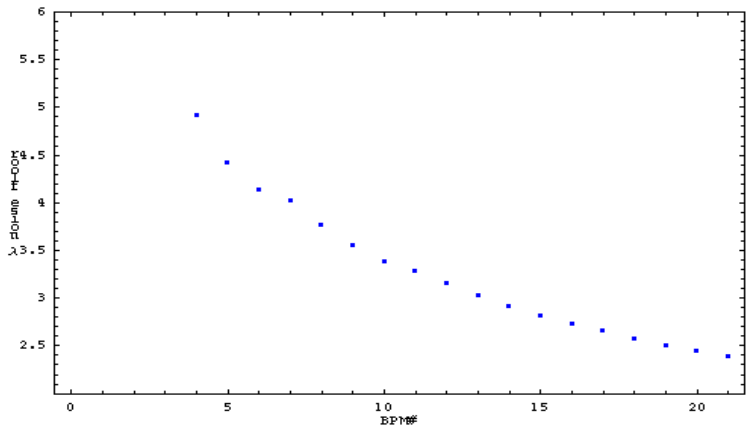


Figure 4-3: Noise floor vs. BPMs number $M$

floor sets up a limitation in our ability to observe beam orbit fluctuations, and can be lowered by increasing $P$ and $M$. All physical variables, which cause a beam trajectory fluctuation above the noise floor, can be observed by this method.

A remarkable usage of these concepts is called "cutting the noise floor." We can remove the noise floor from $B$ by setting the eigenvalues to zero if they are below a certain cut-off (below the noise floor), and then recompute the BPM matrix $\underline{B} = U\underline{\Lambda}V^T$ where $\underline{\Lambda}$ is the new diagonal matrix without a noise floor. Figure 4-4 shows the square root of the variance between $B$-$B_0$ and $\underline{B} - B_0$, here $B_0$ indicates the BPM matrix without BPMs reading noise. From this plot, we can see that the accuracy of BPM readings can be improved by a large factor.

- Distributions of BPMs resolution.

Normally, each BPM have different resolutions. Figure 4-5 shows the noise floor changes for the different distributions of BPMs resolution. So, from

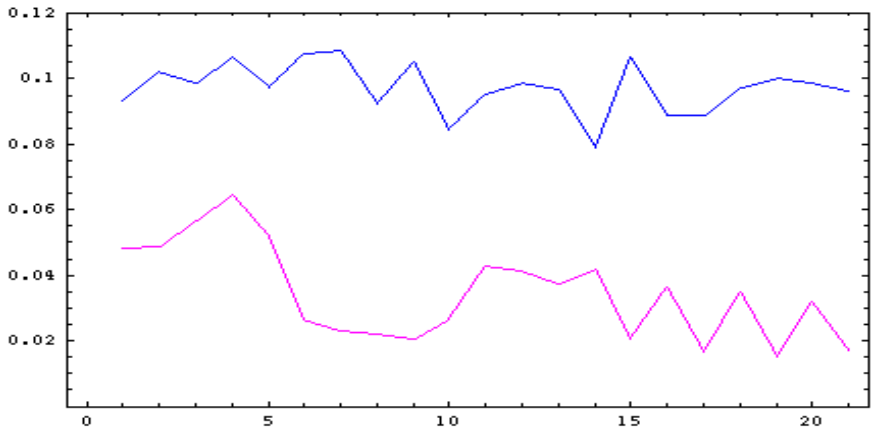


Figure 4-4: Variance between BPM reading and the real beam trajectories

the slope of noise floor, we can roughly estimate the distribution of BPM resolutions.

- Bad BPM.

Now, let us examine the behavior of a bad BPM. In this simulation, a position and angle jitter are created at the beginning of the linac; BPM#14 has a much lower resolution (0.2mm) than others, we call it the bad BPM. We perform an SVD on the B matrix, and we get 3 singular values above the noise floor. For each meaningful singular value, there is a corresponding eigenvector $\vec{v}$ in matrix V. We plot $\vec{v}$, and we call this plot "E.V. plot." Figure 4-6 is the E.V. plot of this example. From this plot, we can see that $\vec{V_3}$ has a big spike at BPM#14, it means that the beam trajectory was changed locally and suddenly, which is physically impossible. So, we know that this BPM must have some problems, and the data from this BPM should also be removed from $B$ before we do any further analysis. This also provide us a method to find bad BPMs along the beam line.

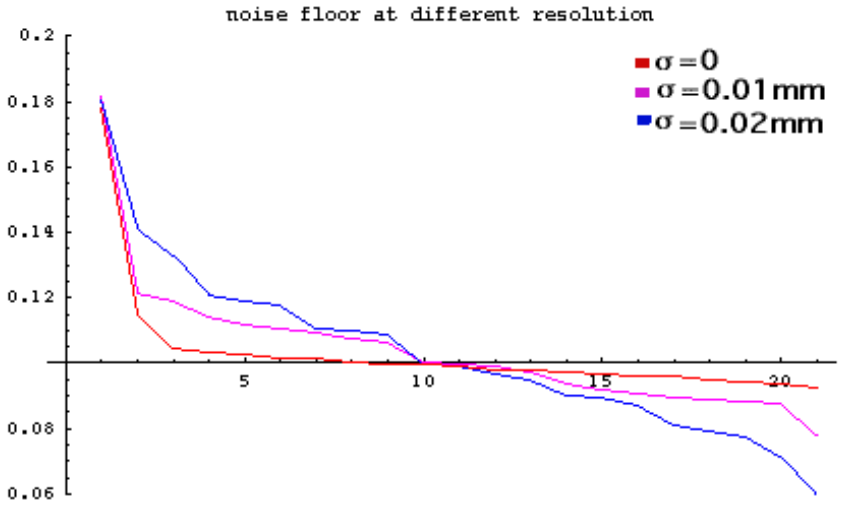


Figure 4-5: Noise floor vs. BPMs resolutions

### 4.3.2 D.O.F analysis

After talking about the BPMs reading noise, we can proceed to our main analysis work. Let us start with a simple example. We suppose that the beam orbit fluctuates due to an $x_0$ and an $x_0'$ injection jitter. Some noise due to a single kicker occured between BPM#16 and BPM#17. Doing SVD on $B$, we find out that there are 3 singular values above the noise floor. In order to locate the sources which cause beam orbit fluctuation, we carry out SVD on part of $B$, and trace the changes of the eigenvalues from the beginning to the end of the beam line, Figure 4-7. This method is called the degree of freedom (D.O.F) analysis. And from this plot, we can see that two physical variables change at the beginning of the beam line, and one physical variable appears between BPM#16 and BPM#17. The result is the same with our simulation conditions, and this means that the beam motion only has 3 measurable degrees of freedom. We call this plot "D.O.F plot." Using this method, we can locate the physical variables which cause the beam trajectory fluctuations.

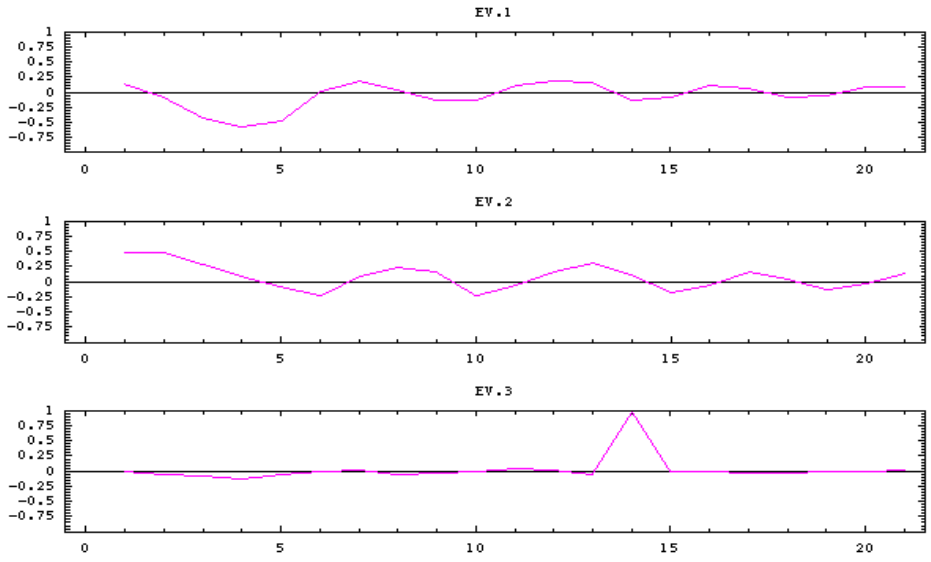


Figure 4-6: Eigenvectors and bad BPM

### 4.3.3 Machine model

In Sect. 2, we declared that, by using the time pattern Q, we can get the corresponding response function of the machine. Now, we will show how to get $Fx$ and $Fx'$ using the first 2 BPMs. Suppose, we know the Twiss parameters between these 2 BPMs i.e. $m_{11}^{1\to 2}$ and $m_{12}^{1\to 2}$, then we can use $\hat{x}_1$ and $\hat{x}_2$ to build the time pattern $\mathrm{Q}(\hat{x}_1, \hat{x}_1')$. $Fx$ and $Fx'$ can be gotten from Eqs. (2.10). The results are shown in Figure 4-8. $m_{11}$ and $m_{12}$ are the machine model which are used in the simulation. From these figures we can see that:

1. We *do* can get a realistic machine model from the BPM reading matrix;

2. The accuracy can be improved seriously by cutting the noise floor.

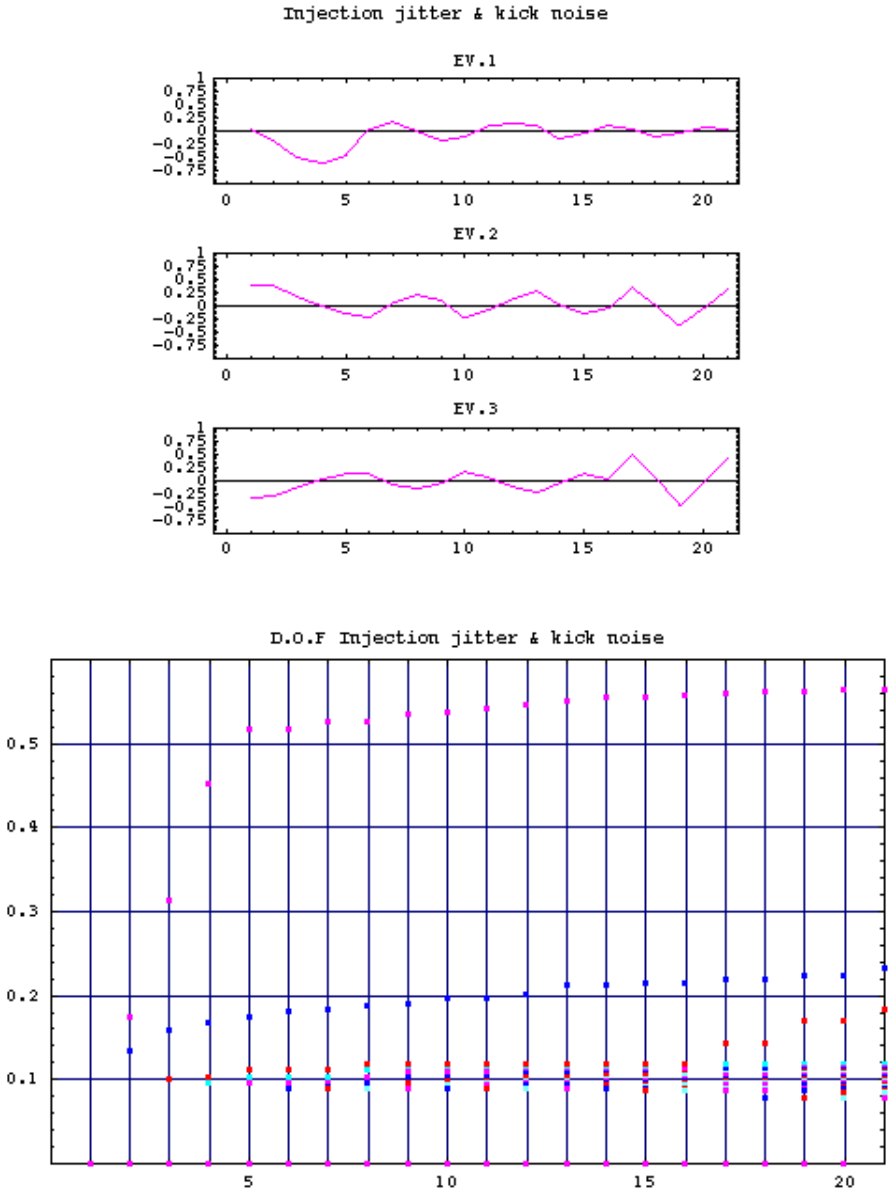


Figure 4-7: Injection jitter and kicker noise

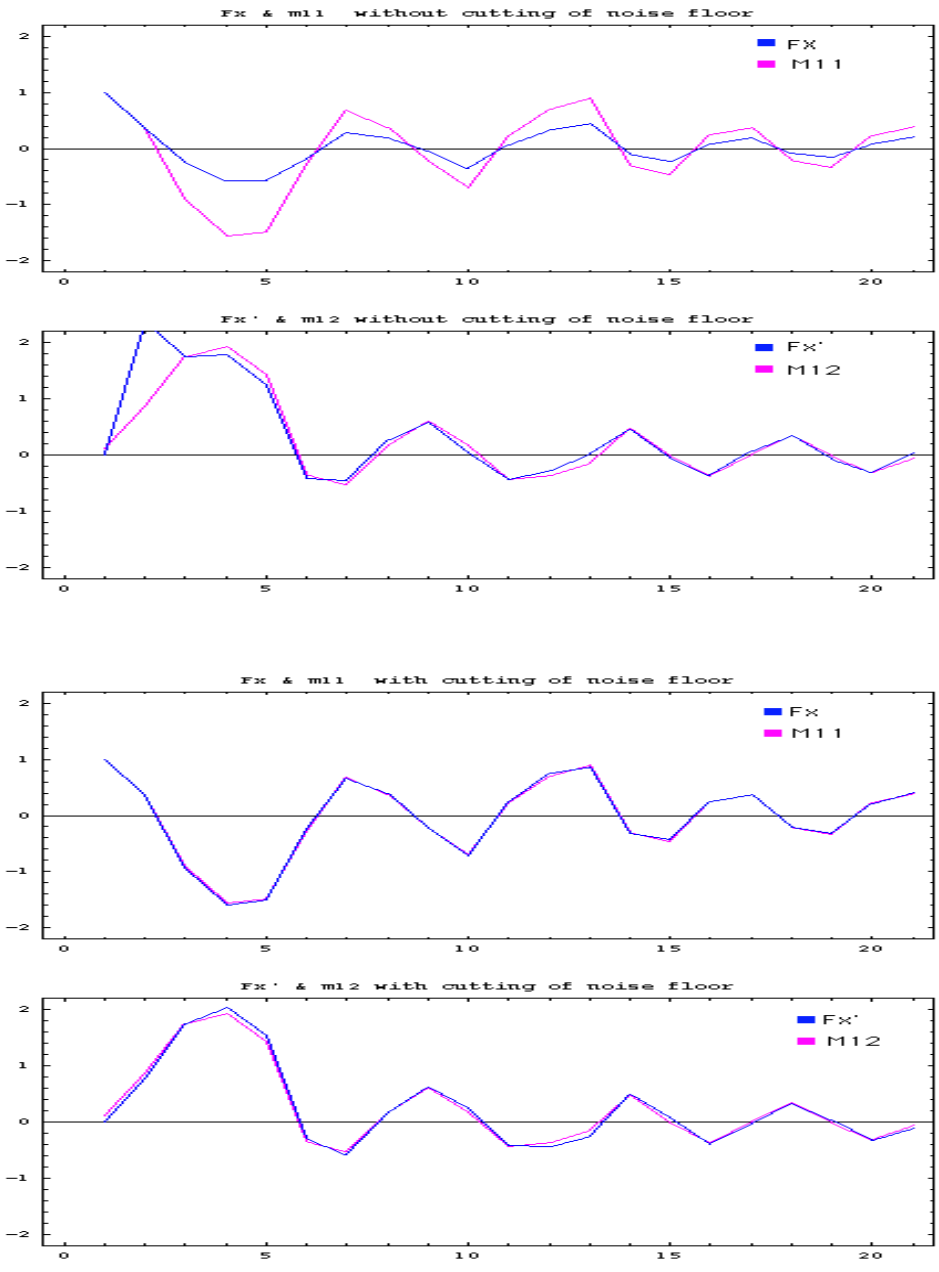


Figure 4-8: Calculated machine model without/with cutting the noise floor

### 4.3.4 Energy jitter

In this case, the incoming beam has 3 free parameters $x_0$, $x_0'$, and $\Delta\delta = 2.5\%$. Figure 4-9 and Figure 4-10 show the D.O.F plot, E.V. plot and machine model for this case. From the D.O.F plot, we can see that for our BPMs resolution (0.1mm), such an energy jitter is hard to observe.

### 4.3.5 More general case

In this example, we simulate the beam with an injection jitter ($x_0$, $x_0'$, and $\Delta\delta = 2.5\%$), one quadrupole with 0.1% field ripple, one dipole field ripple and one accelerating structure with an accelerating phase oscillation of $\Delta\phi = 5^0$. Figure 4-11 and Figure 4-12 show the simulation results. From these results, we can conclude that the beam is not sensitive to the rf phase oscillation, quadrupole magnet ripple and energy jitter.

The bunch length and beam current do not affect the free betatron oscillation in the absence of wakefields. Also the misalignment does not make beam orbit fluctuations in the absence of wakefield effects.

A remarkable thing which need to be mentioned here is the machine model gotten from the B matrix. When we take off the noise floor, it agrees well with the ideal one which we used in the simulation. Also it is **damped** along the beam line. It is easy to get an understanding of this phenomenon: the normalized emittance keep constant while the beam energy increases, it leads to damping of the amplitude of the beam oscillations.

## 4.4 Wakefields

Now, we discuss the beam simulations with wakefields. The KEKB injector linac works in a single bunch mode and the bunch length is about 3mm.

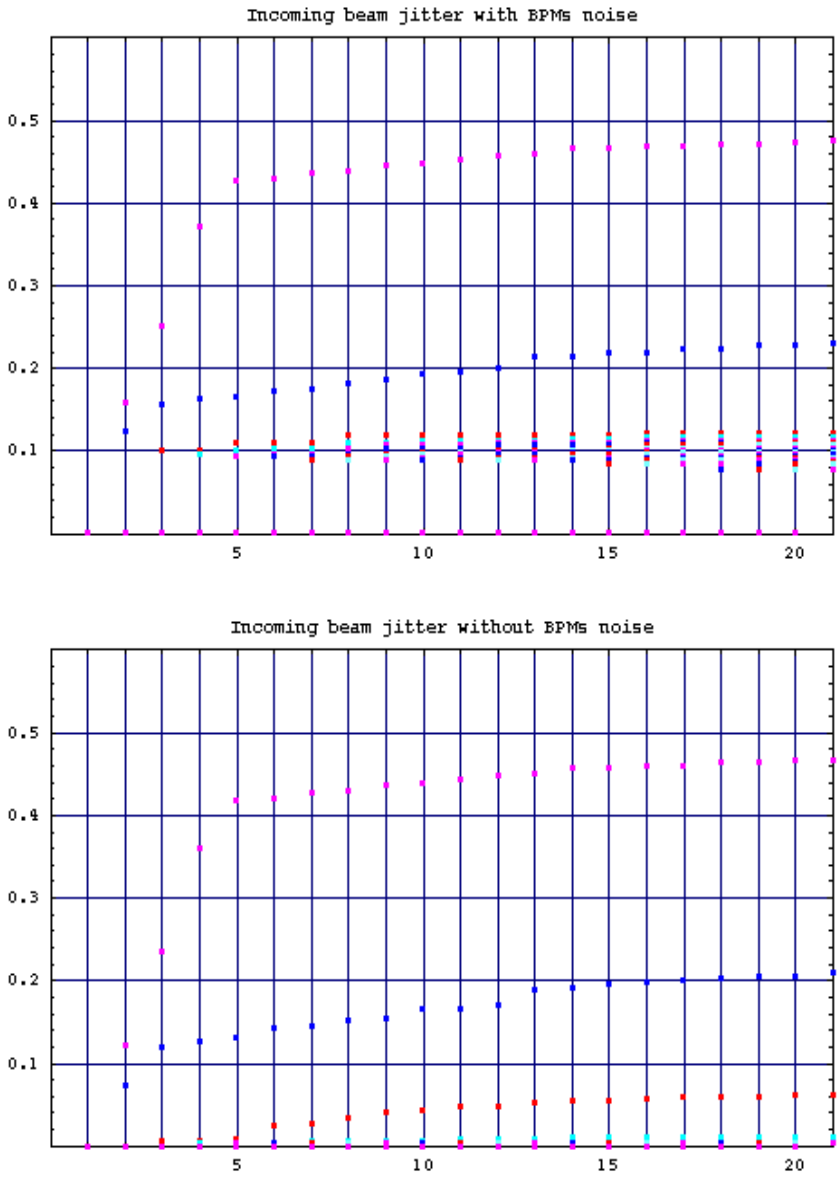


Figure 4-9: Incoming beam jitter: $x_0$, $x_0'$, and $\Delta\delta = 2.5\%$

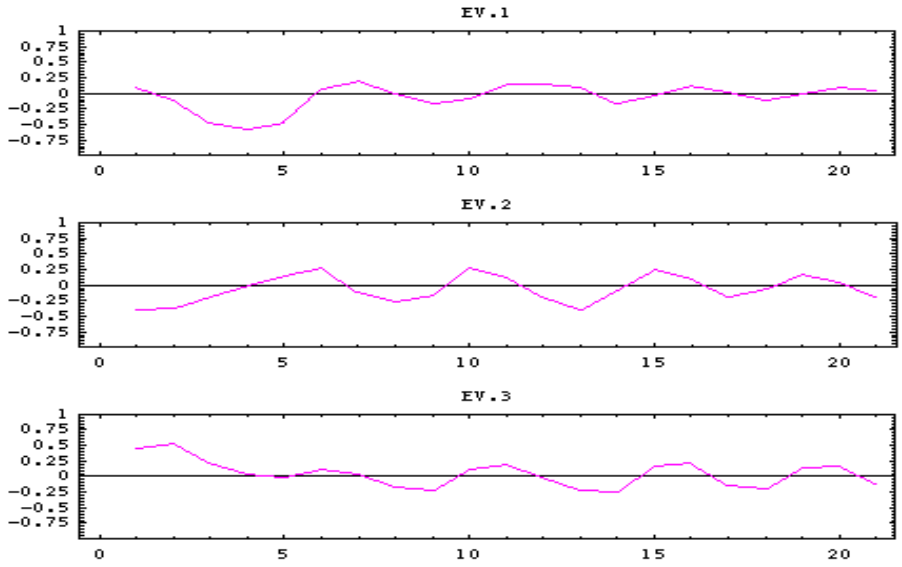


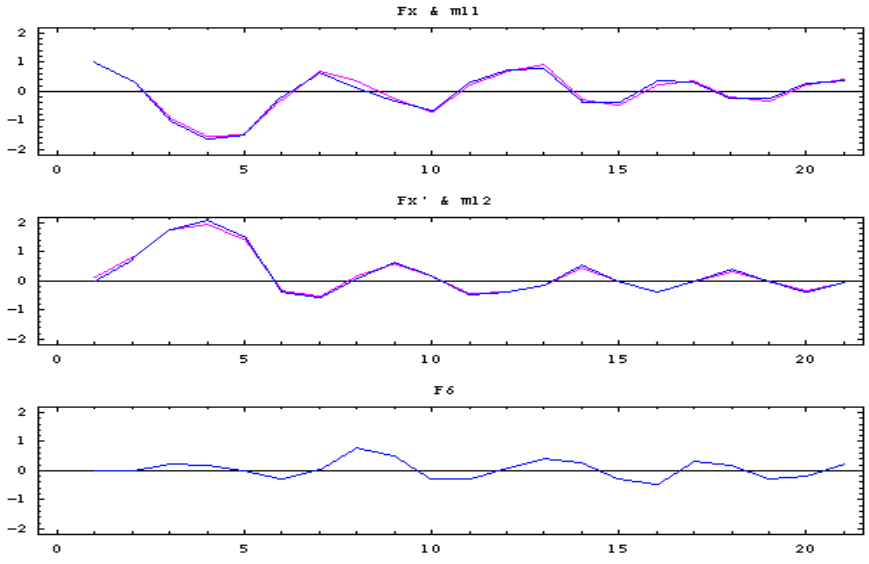


Figure 4-10: Incoming beam jitter: $x_0$, $x_0'$, and $\Delta\delta = 2.5\%$

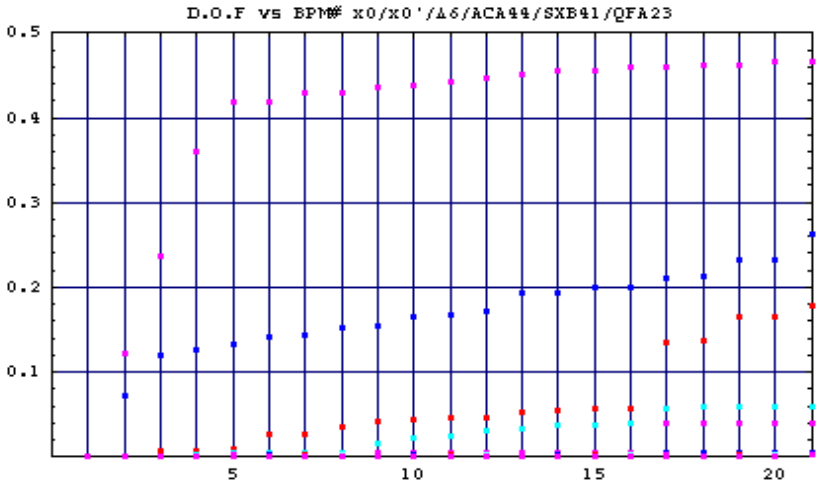


Figure 4-11: Incoming beam jitter:$x_0$, $x_0'$,$\delta = 2.5\%$, magnet ripple and $\Delta\phi$

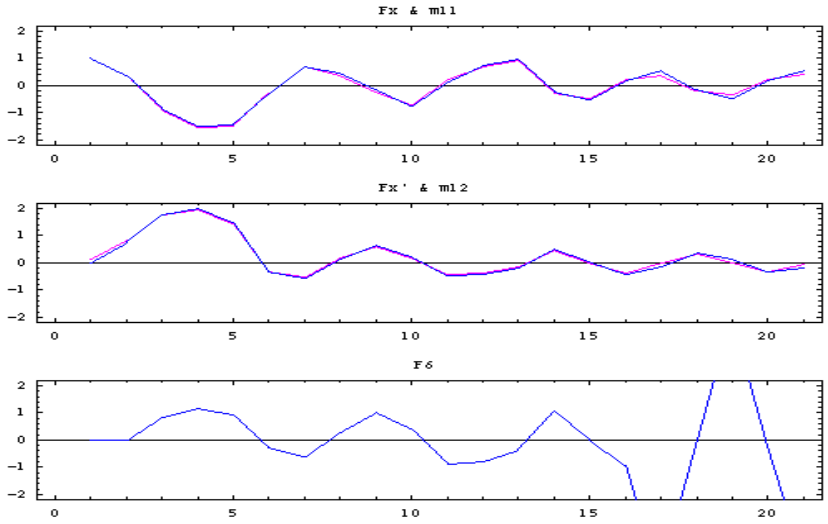

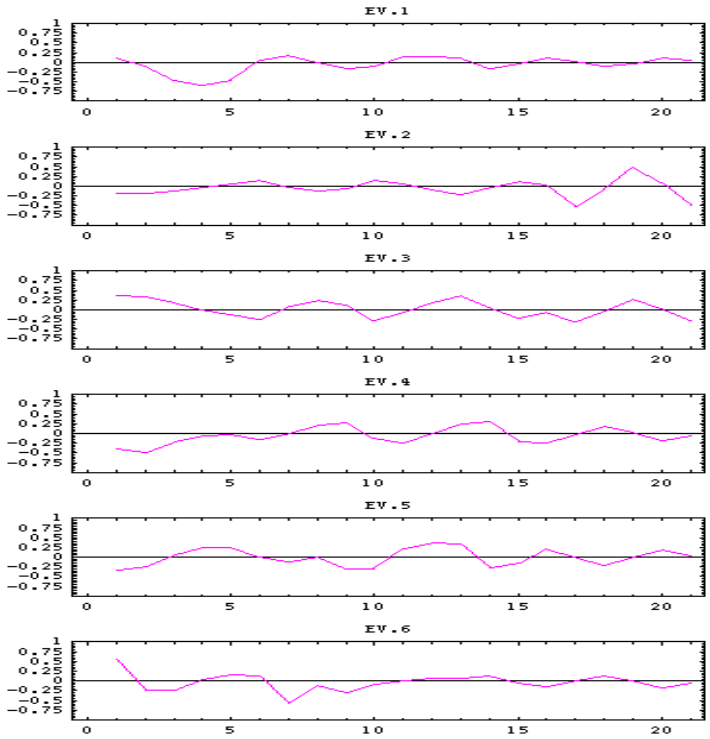


Figure 4-12: Incoming beam jitter:$x_0$, $x_0'$,$\delta = 2.5\%$, magnet ripple and $\Delta\phi$

### 4.4.1 Short-range wake functions

For short-range wakefields, we can use some simplified formulas to calculate the wake functions. The formulas we use here are given by K.Yokoya [35] as following: For the longitudinal wake,

$$W_L(s) = \frac{cZ_0}{\pi a^2}\left[1 + W_{L1}\sqrt{\zeta} + W_{L2}\zeta + W_{L3}\zeta\sqrt{\zeta}\right] \tag{4.1}$$

and for the transverse wake,

$$W_T(s) = \frac{cZ_0}{\pi a^4}s\left[2 + W_{T1}\sqrt{\zeta} + W_{T2}\zeta + W_{T3}\zeta\sqrt{\zeta}\right] \tag{4.2}$$

where $Z_0 = 377\Omega$ is the impedance of vacuum, and

$$\zeta = \frac{Ls}{a^2}$$

with: $L$ =cavity cell period, $a$=iris aperture.
The coefficients are given by:

$$\begin{array}{lllllll} W_{L1} & = & -1.614r^{0.122} & W_{L2} & = & 1.012r^{0.169} & W_{L3} = -0.231r^{0.111} \\ W_{T1} & = & -2.781r^{0.217} & W_{T2} & = & 1.637r^{0.511} & W_{T3} = -0.364r^{0.793} \end{array}$$

where

$$r = \frac{a/\lambda}{0.15}$$

with $\lambda$ = wave length. These formulas are valid when the following conditions are satisfied:

$$\begin{gathered} 0.10 \le a/\lambda \le 0.20 \\ 0.15 \le d/L \le 0.25 \\ 0 \le s \le 0.2L \end{gathered}$$

$d$ is the thickness of the disk.

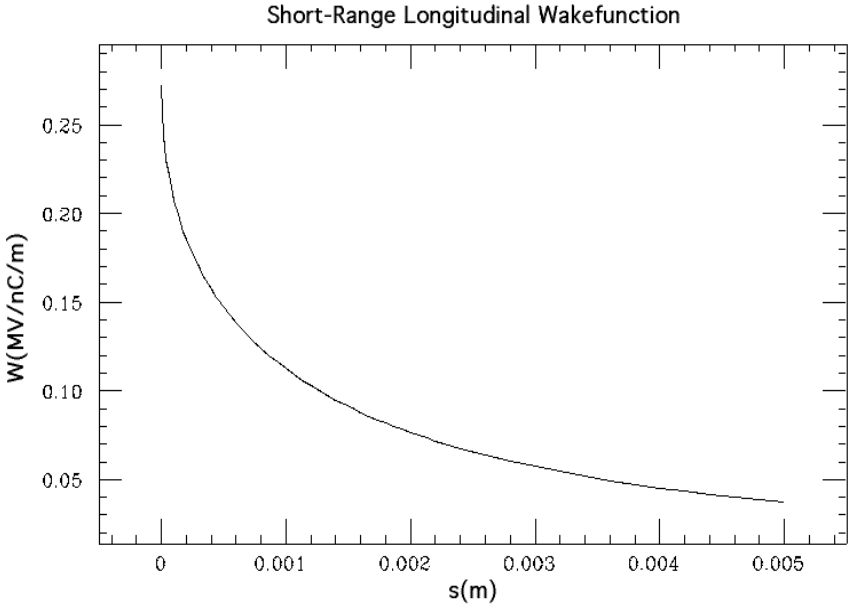


Figure 4-13: Longitudinal wake function for KEKB injector linac

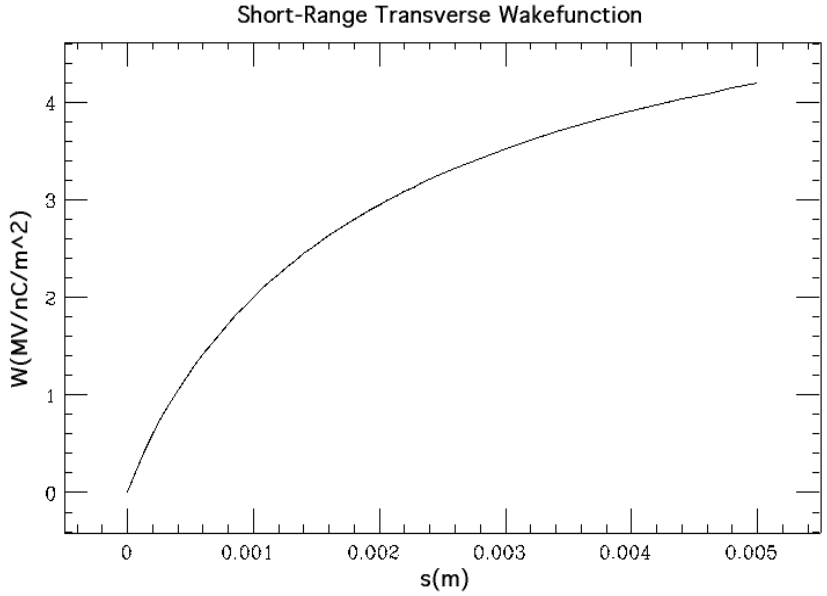


Figure 4-14: Transverse wake function for KEKB injector linac

For KEKB injector: $L = 34.98mm,\ a = 11.5mm,\ \lambda = 104.97mm$ The longitudinal and transverse wake functions are shown in Figure 4-13 and Figure 4-14 respectively.

We add these two wake functions to our accelerator structures. When the beam passes through them, the wakefields are established and act back on the beam itself. In our simulation, the beam has a Gaussian distribution in the $z$ direction. It has been spliced into $J = 100$ macro particles that have the same charge. An arbitrary macro particle $j$ $(j = 1, \cdots, J)$ gets a transverse momentum kick, $\Delta p_x$, when it passed through an accelerating structure:

$$\Delta p_x(j) = \sum_{i=1}^{j} \frac{Ne}{J} w_T(z_j - z_i) L_{cav} x(i) \ \ (eV) \tag{4.3}$$

where $L_{cav}$ is the length of one accelerating structure. The centroid beam position and angle are:

$$\overline{x} = \frac{1}{J}\sum_{i=1}^{J} x(i) \qquad \overline{x}' = \frac{1}{J}\sum_{i=1}^{J} x'(i)$$

The transverse emittance at position $s$ is given by:

$$\varepsilon_{wake} = \sqrt{\left\langle x^2 \right\rangle \left\langle x'^2 \right\rangle - \left\langle xx' \right\rangle^2} \tag{4.4}$$

where

$$\begin{aligned}
\left\langle x^2 \right\rangle &= \frac{1}{J}\sum_{i=1}^{J}\left(\beta_x(i)\frac{\varepsilon_0\gamma(0)}{\gamma(s)} + (x(i) - \overline{x})^2\right) \\
\left\langle x'^2 \right\rangle &= \frac{1}{J}\sum_{i=1}^{J}\left(\gamma_x(i)\frac{\varepsilon_0\gamma(0)}{\gamma(s)} + (x'(i) - \overline{x}')^2\right) \\
\left\langle xx' \right\rangle &= \frac{1}{J}\sum_{i=1}^{J}\left(-\alpha_x(i)\frac{\varepsilon_0\gamma(0)}{\gamma(s)} + (x(i) - \overline{x})(x'(i) - \overline{x}')\right)
\end{aligned} \tag{4.5}$$

The emittance growth rate $R$ is defined as:

$$R = \varepsilon_{wake}(s)\,\gamma(s)\,/\varepsilon_0\gamma(0) \tag{4.6}$$

For more detail discussion of this topic please see the appendix. From the discussion in the previous section, we know that the emittance dilution is almost proportional to the square of the beam current.

### 4.4.2 Misalignment effects

When the beam passes through a misaligned accelerator structure, a transverse wakefield will be excited. The wakefield acts back to the beam and causes an emittance dilution. Here we illustrate the misalignment effects by a simple example, and explain how to use MIA to find out the location of the structure misalignment and how to get the emittance growth rate from the BPM reading matrix.

The simulation conditions are as following:

1. Betatron injection jitter $\Delta x_0 = 10\mu m$, $\Delta x_0' = 10\mu rad$.
2. 10% current jitter ($I_0 = 10nC$).
3. 10% bunch length jitter ($\sigma_z = 1.5mm$).
4. Incoming phase jitter $\Delta\phi_{inj} = 2.5^0$.
5. One structure misalignment ($300\mu m$) within KEKB injector lattice (BPM#5-BPM#6).

We generated a 2500 pulses BPMs data set for analysis. Having done an SVD on the data set, we obtained the D.O.F plot and E.V. plot (see Figure 4-15). Suppose we can measure all of the parameters ($x_0$, $x_0'$, $I$, $\sigma_z$, and $\Delta\phi_{\text{inj}}$), then we can use the time pattern decomposition method to get the machine model. Figure 4-16 is the machine model calculated from our initial simulation data.

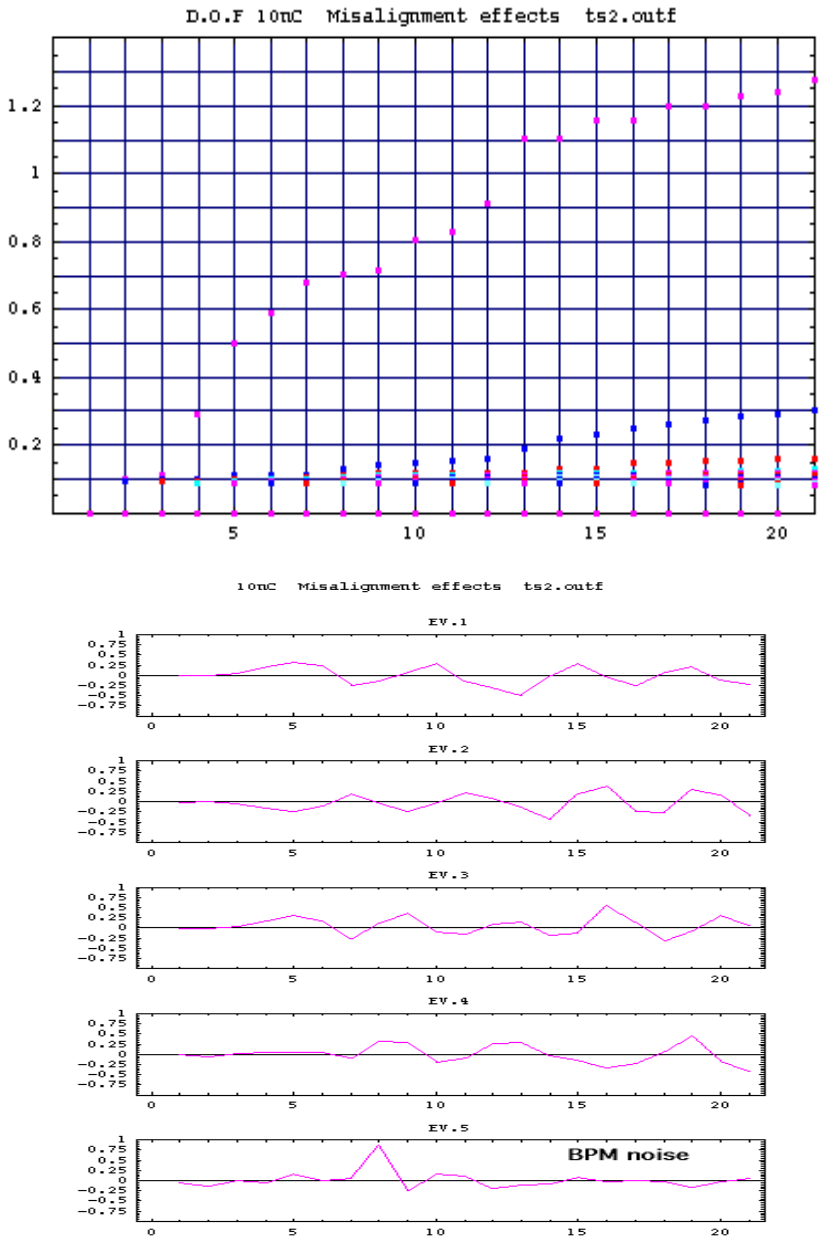


Figure 4-15: Misalignment effects: High beam current

From this figure we see that only betatron jitters are important to the beam orbit fluctuation. Also in a real case, the measurements of these parameters always have errors, and these errors will be brought into our calculations of the machine model. But for betatron motion, because we can use the technique of cutting of noise floor, the model is more accurate. Figure 4-16 also gives the machine model calculated from $B$ (pink line). From these figures we also get the amplitude of eigenvectors and machine model ($Fx$, $Fx'$) increasing along the beam line. It implies the existence of emittance dilution. The emittance dilution along the linac is shown in Figure 4-17. The results can be compared with the low beam current case ($I_0 = 1nC$), see Figure 4-18. From this result, we can conclude that when current is low, the beam is not sensitive to the misalignment effects, the beam behavior is more like a free betatron oscillation. The same results can be obtained with other simulation conditions.

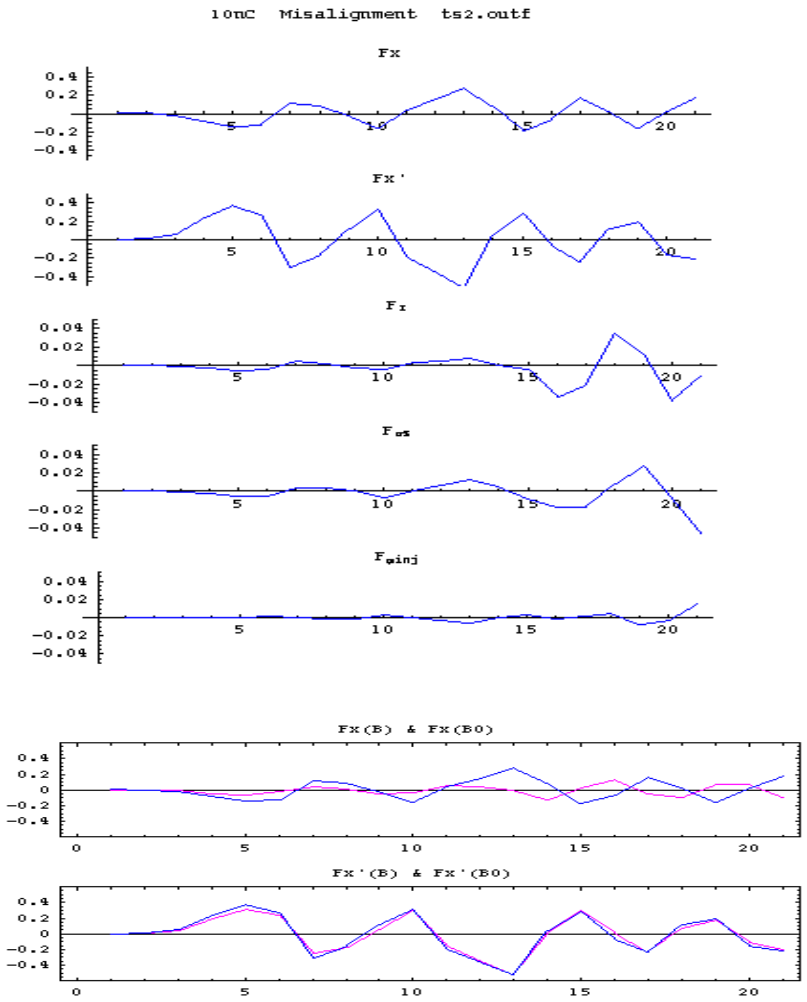


Figure 4-16: Misalignment effects: High beam current-Machine model

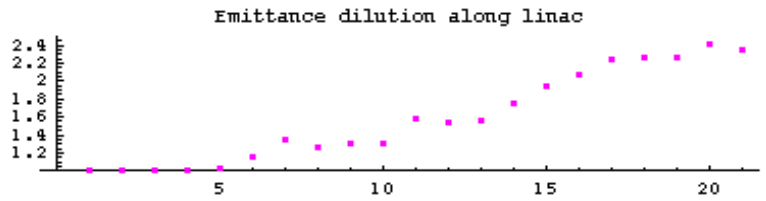


Figure 4-17: Misalignment effects: High beam current-Emittance dilution

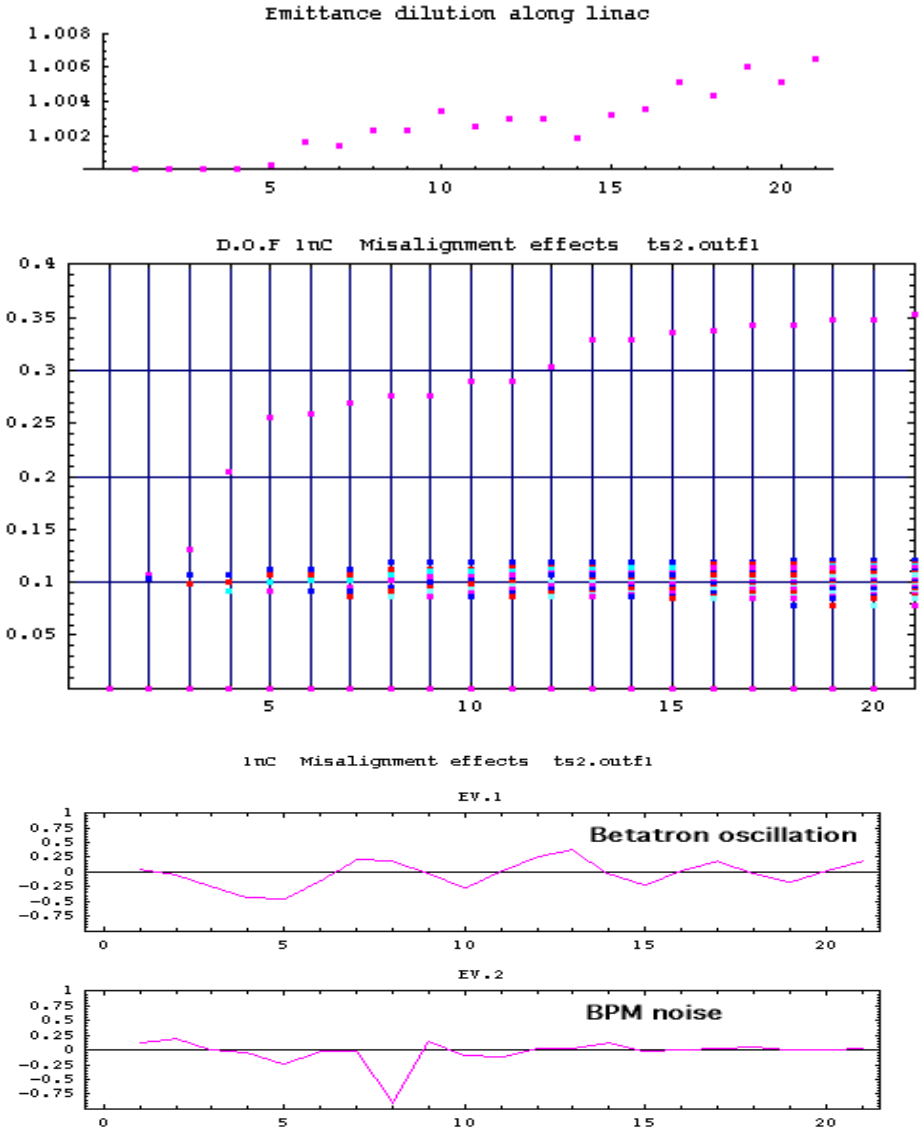


Figure 4-18: Misalignment effects: Low beam current ($\delta x_0 = 40\mu m$, $\delta x_0' = 40\mu rad$)

### 4.4.3 Injection offset

When the beam is injected into the linac with some offset (it always true in the real case), it will excite betatron oscillations everywhere. As a result, the transverse wakefield is excited and acts back on the beam. The betatron oscillation is enlarged by the wakefield effects, and this causes emittance dilution. Now, we start to simulate it with an injection offset $x_0 = 50\mu m$, other simulation conditions are the same as before except that no structure misalignments are present. The simulation results are shown in Figure 4-19 and Figure 4-20. From these results, we can conclude that:

1. when the beam current is low, the beam behavior is just like the free betatron oscillation, the emittance does not dilute too much, and we can use it to reveal or check our initial lattice design.

2. when the beam current increases, the wakefields effects dominate the beam behavior. For different beam orbits, the machine model is also different. This phenomenon also provides us one method to alleviate wakefields effects by orbit steering.

3. the amplitude of the eigenvector is damped along the linac when the wakefield is weak, but it is increased when the wakefield is strong. We can estimate the emittance dilution from this phenomenon.

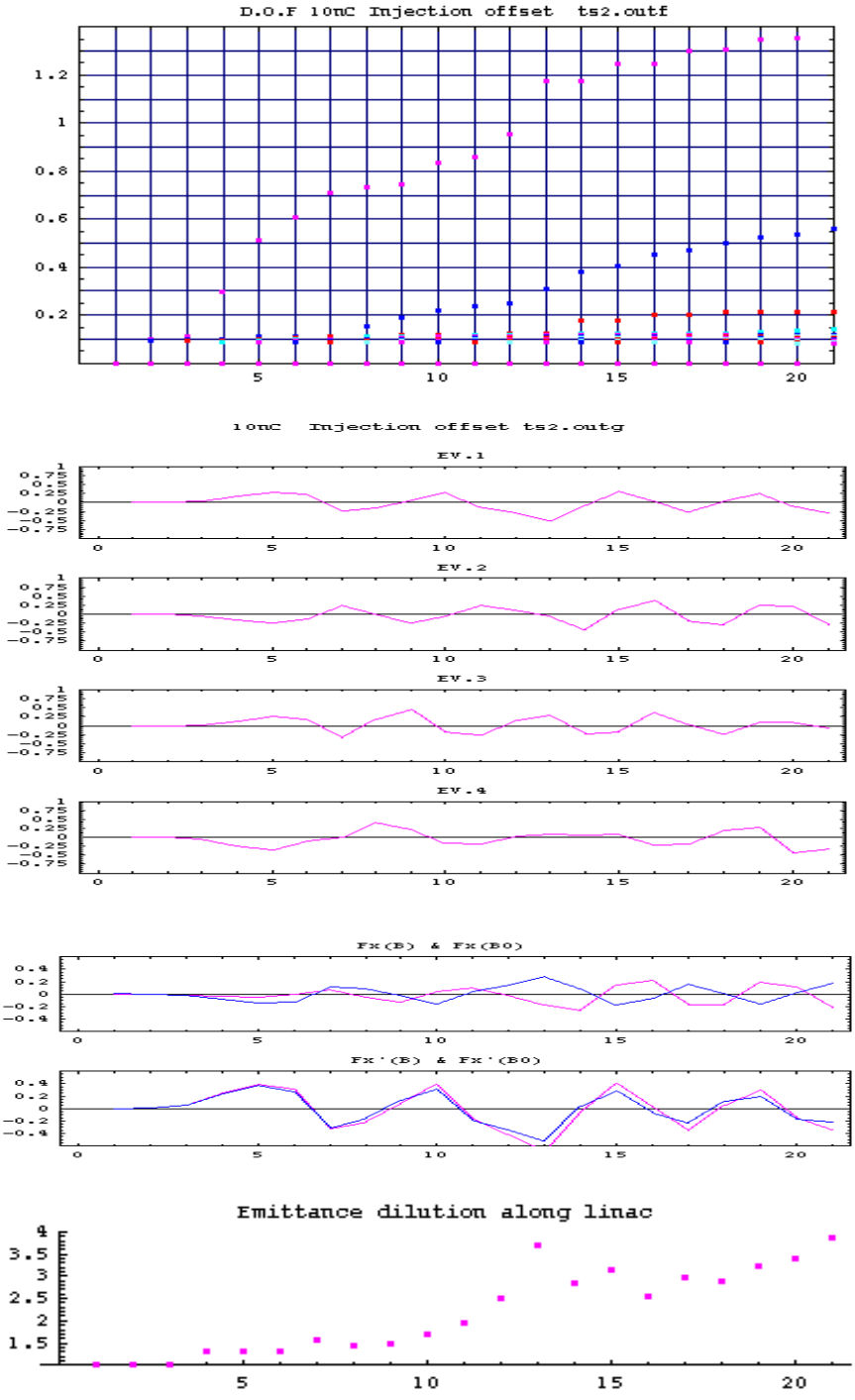


Figure 4-19: Injection offset effects: High beam current

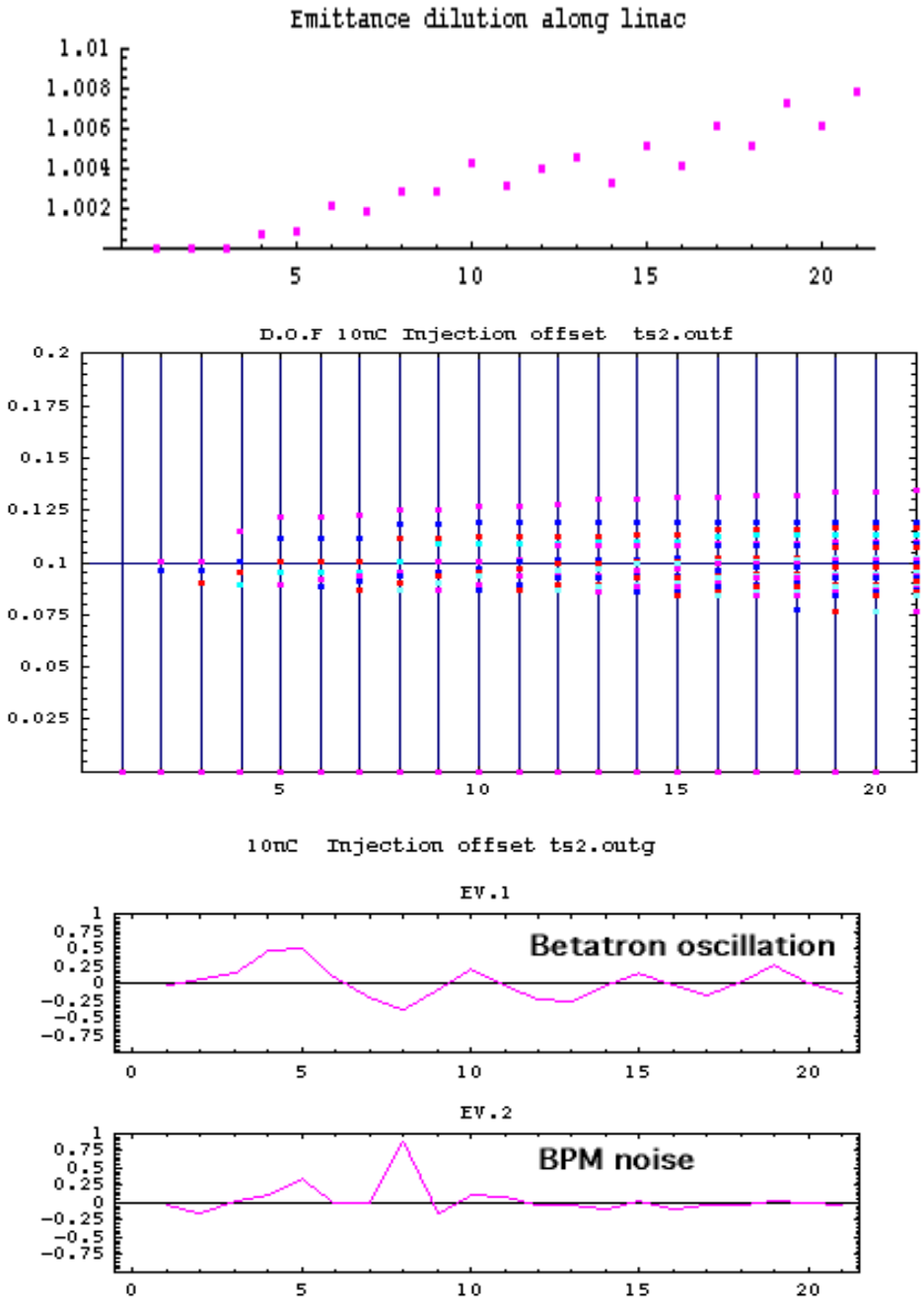


Figure 4-20: Injection offset effects: Low beam current

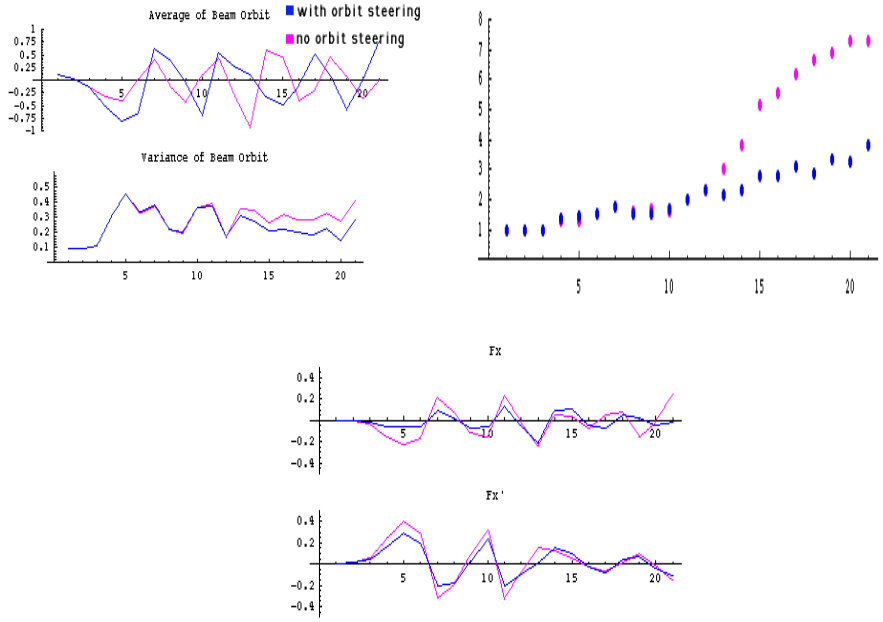


Figure 4-21: Orbit steering: emittance dilution and machine model

### 4.4.4 Orbit steering and Lattice re-matching

From the previous simulation results, we have already seen that for $50\mu m$ injection offset only the emittance dilution is already a factor of 4. From Figure 4-19 we can see that most of the emittance dilution occurs between BPM#10 and BPM#15. In order to alleviate the emittance dilution, first we need to produce an orbit correction or a steering. We'll show how this works. We assume the injection offset is $100\mu m$, other simulation conditions are the same with before. Figure 4-21 shows the results of emittance dilution and machine models getting from the BPMs reading matrix for the different beam orbit. The red line is without orbit steering, the blue line is with orbit steering. Figure 4-22 shows the D.O.F analysis for these two cases.

The another thing we can do is to re-match the lattice. We have seen that the emittance dilution happened near BPM#13, also from Figure 4-1 we can

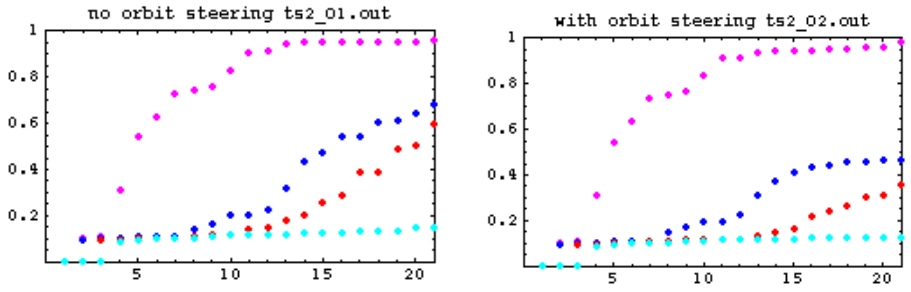


Figure 4-22: Orbit steering: D.O.F analysis

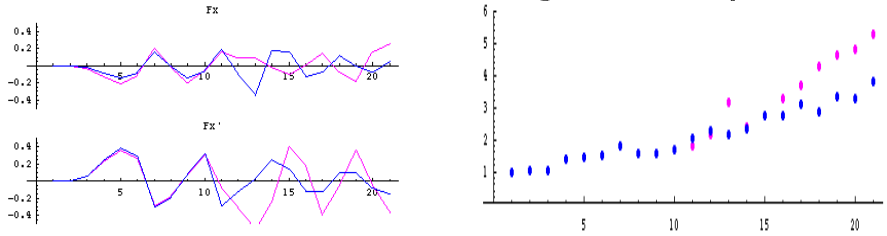


Figure 4-23: Re-matched lattice: Machine model and emittance dilution along the linac

see a sharp beta-function increase occurs around there. From Eq.3.16, we know that the emittance dilution is proportional to the square of the beta-function. So, trying to re-match the lattice becomes another way to alleviate the emittance dilution. Figure 4-25 shows the new lattice, and Figure 4-23 and Figure 4-24 show the results of simulations compared with the previous cases.

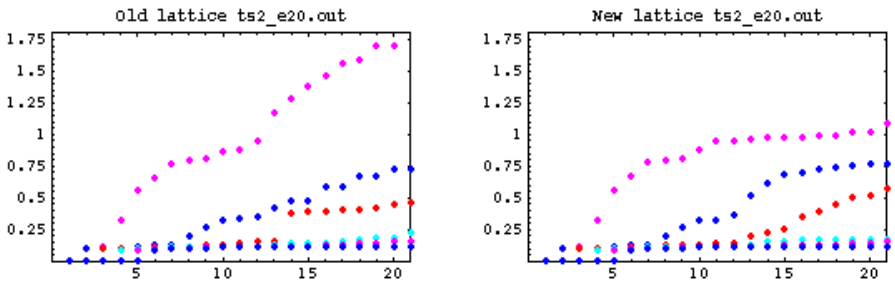


Figure 4-24: Re-matched lattice: D.O.F analysis

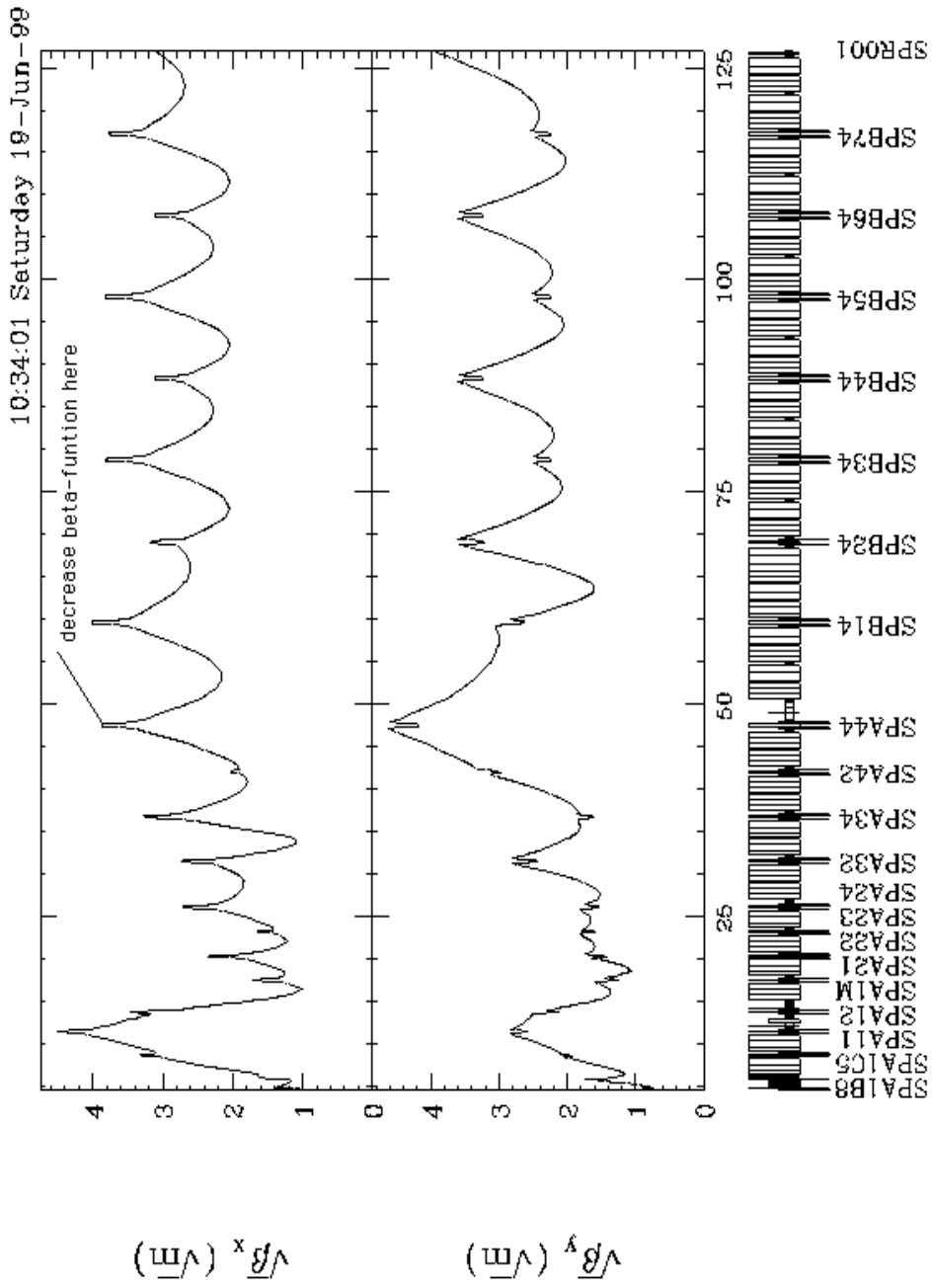


Figure 4-25: Beta-function of re-mached lattice

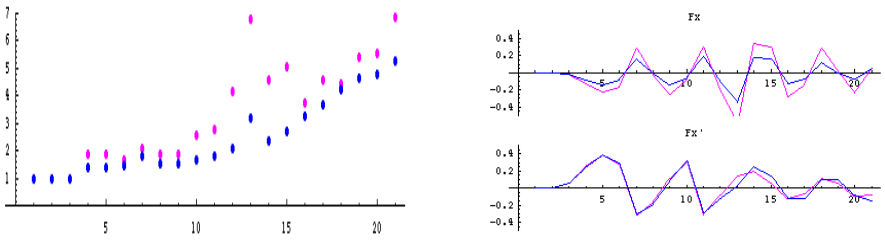


Figure 4-26: BNS damping: Machine model and emittance dilution along the linac

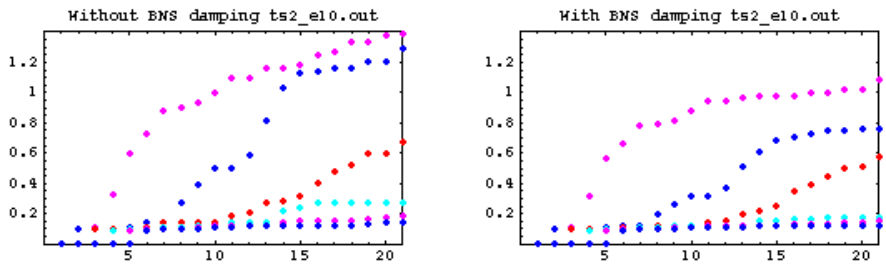


Figure 4-27: BNS damping: D.O.F analysis

### 4.4.5 BNS damping

In Section 3 we talked about BNS damping to alleviate emittance dilution. We assume that a correlated energy spread within the bunch is about 20% when the beam just leave the buncher, and we make sure that the energy of the tail particles is less than the energy of the head particles. We compare the simulation results between no correlated energy spread and with correlated energy spread. From the results we can see that with the BNS damping, the emittance dilution can be reduced. The machine model and emittance dilution along the linac are given in Figure 4-26; Figure 4-27 shows the D.O.F analysis results.

The wakefield effects can be found by MIA, and we also see the difference between various machine models. For practice usage of this method, we need to do more careful work.

# 5 Experimental results

The experiments were done for two cases: low beam current (around 1nC/bunch) and high beam current (around 10nC/bunch). During the experiments, we recorded the BPMs data and the beam current for the same pulses. For a later reference to the machine status, all magnets' power supply and klystrons status were also recorded during the experiments. Because of limitations in data collection, these data were not recorded pulse by pulse. As in the simulations, in a stable operating run, the beam is not sensitive to those parameters.

We show 4 typical experimental results in this thesis:

1. Mar.23 20:21:45 1nC 1980 pulses.
2. Mar.27 17:38:56 1nC 1100 pulses.
3. Mar.23 17:26:25 10nC 1500 pulses.
4. Mar.30 13:54:09 10nC 2600 pulses.

In order to compare them with each other, we put the same kind of plots together. Figure 5-1 shows the average beam orbits (it should also include the BPMs offset). Figure 5-2 shows the square root of the variance of the beam orbits. Figure 5-3 and Figure 5-4 show the results of D.O.F analysis of the BPM reading matrix.

One thing should be emphasised here: these experiments were done when the KEKB injector linac was injecting beam into KEKB storage ring. That means that our method is totally **non-invasive**!

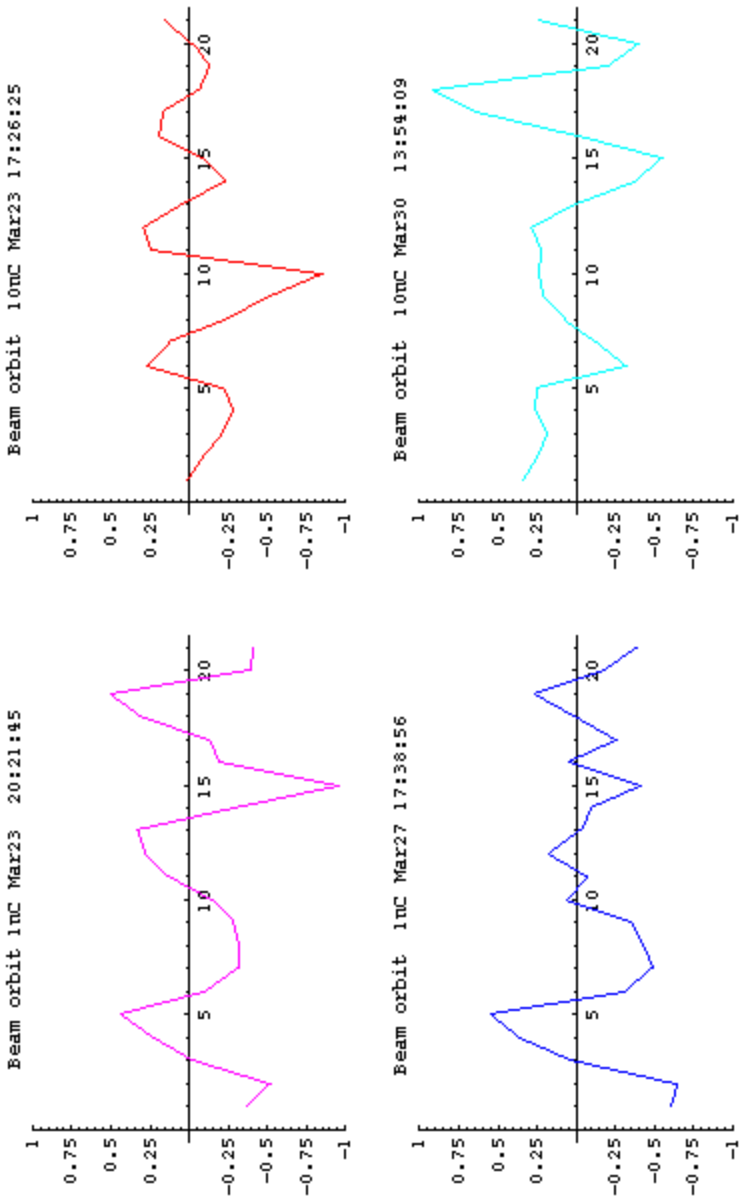


Figure 5-1: Exp.: The average beam orbit

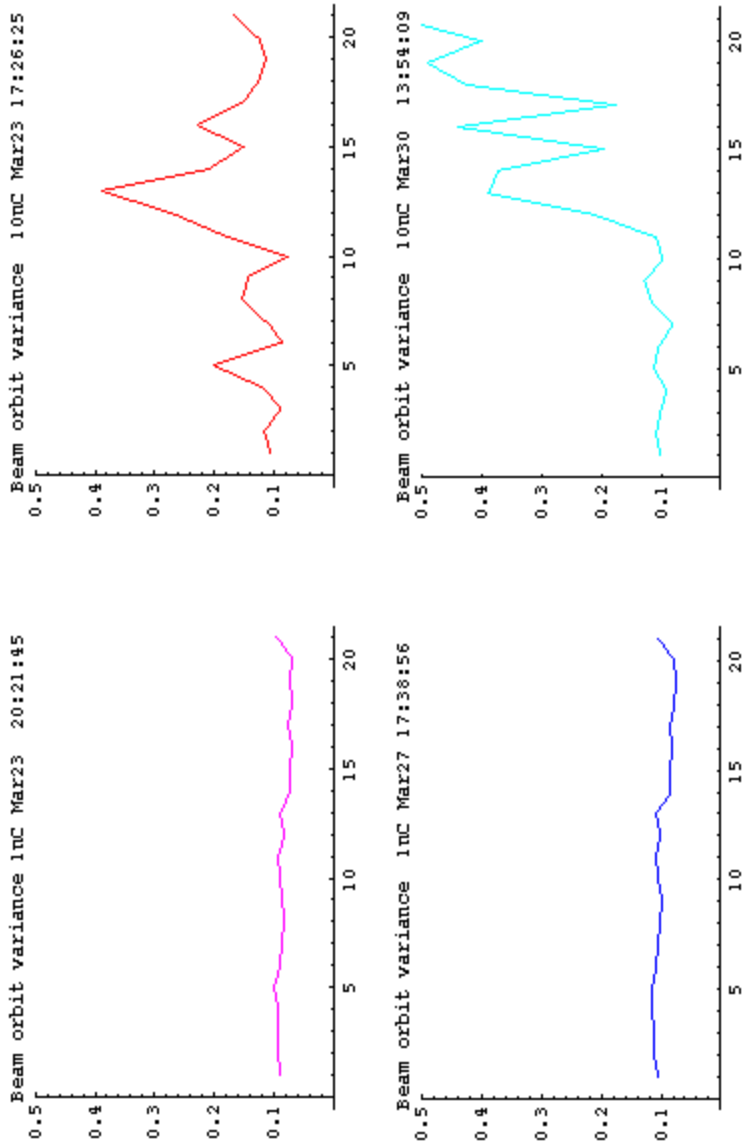


Figure 5-2: Exp: Square root of the variance of beam orbits

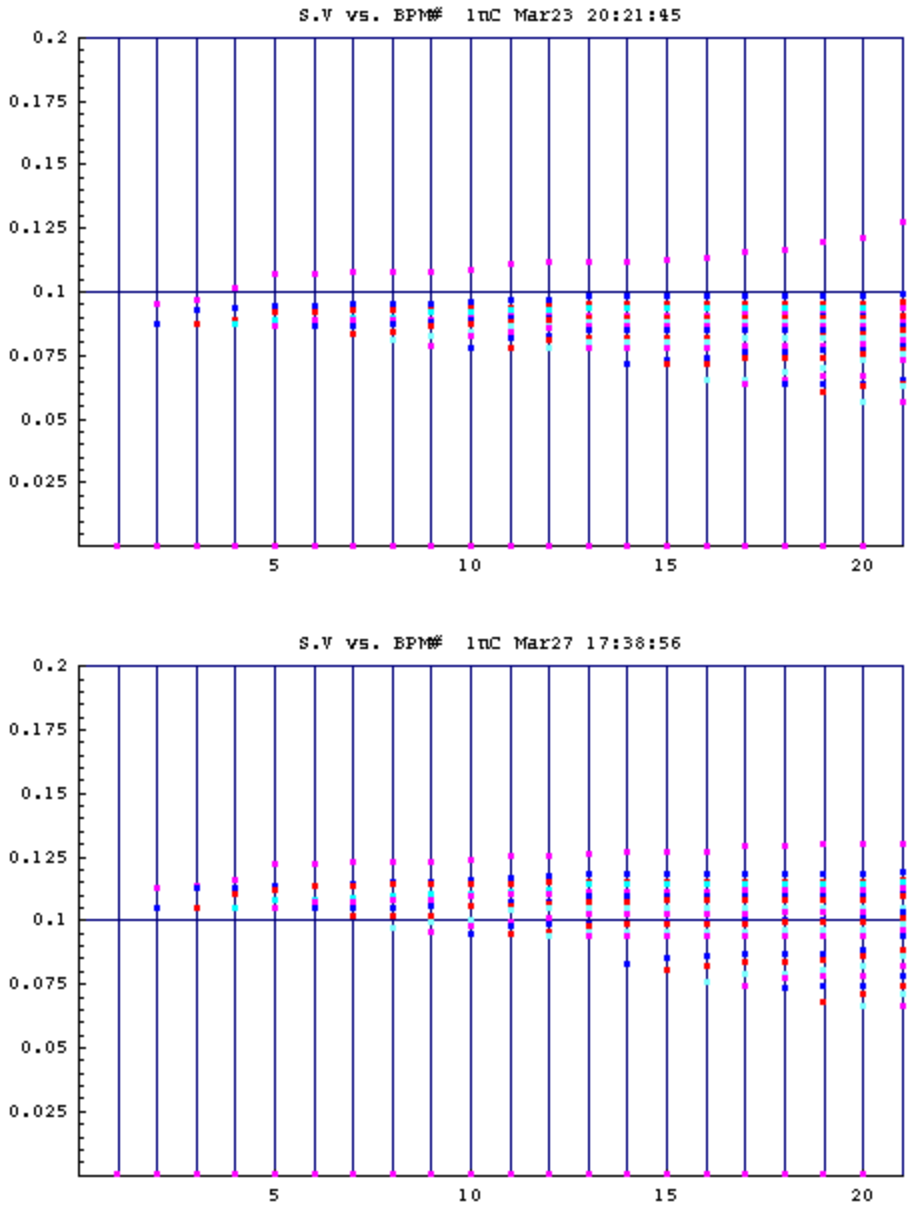


Figure 5-3: Exp: D.O.F analysis at low beam current

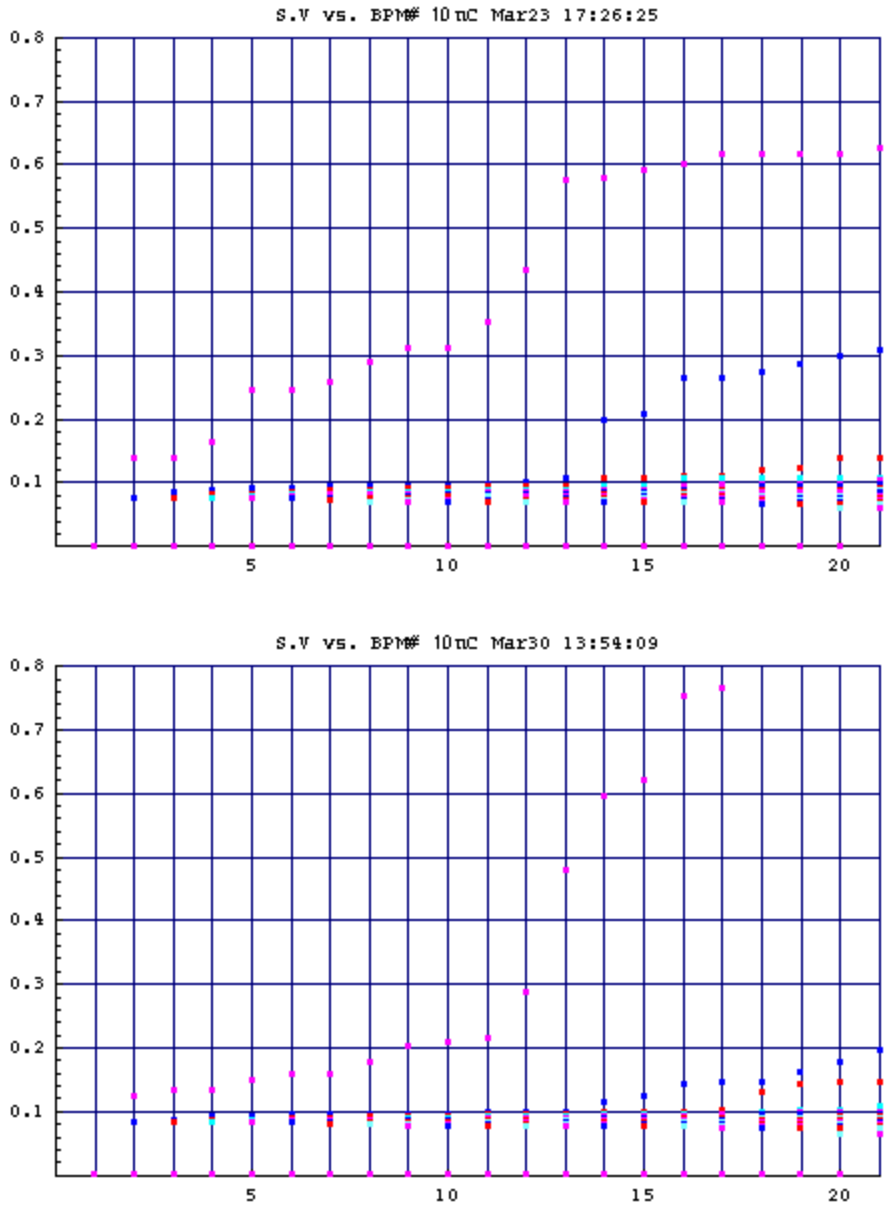


Figure 5-4: Exp: D.O.F analysis at high beam current

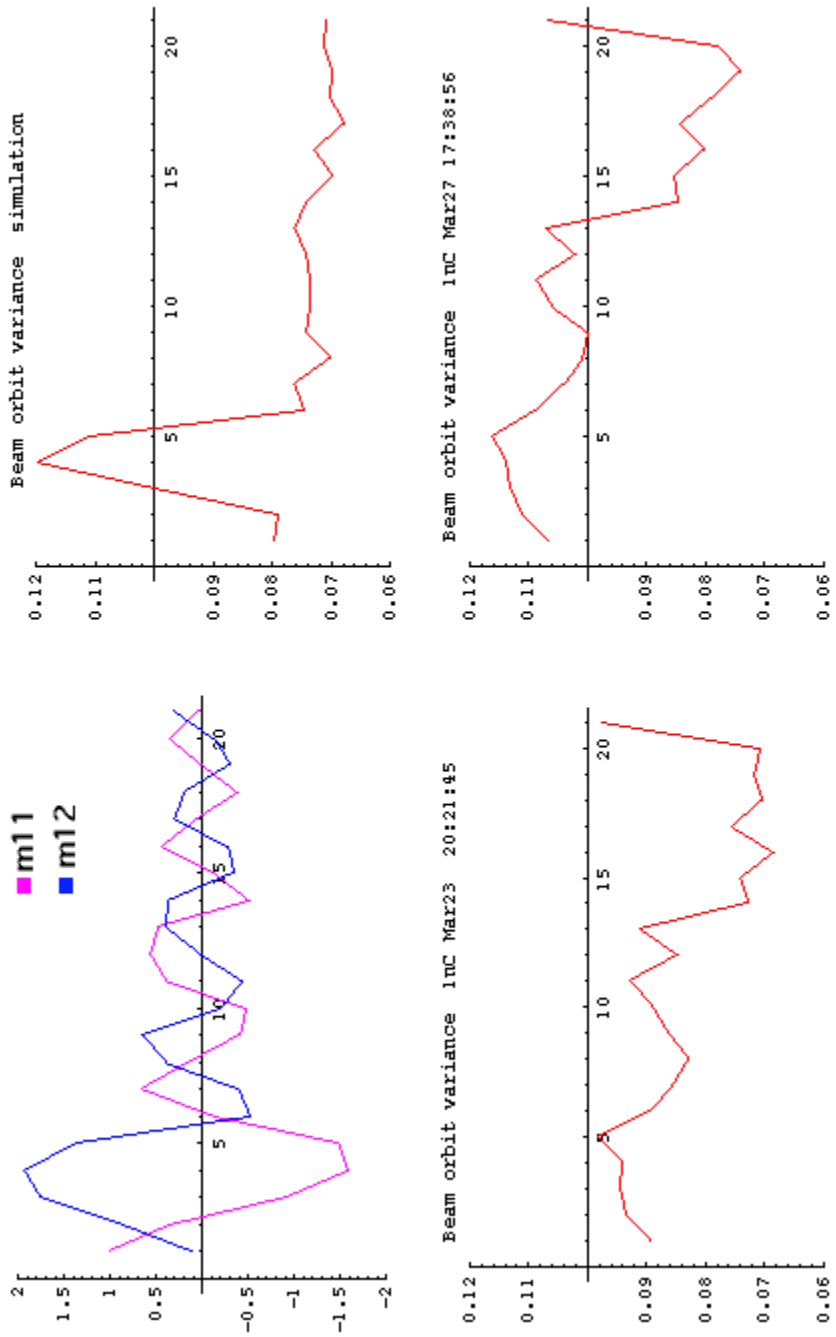


Figure 5-5: Exp: Machine model (ideal) and variance of beam orbits

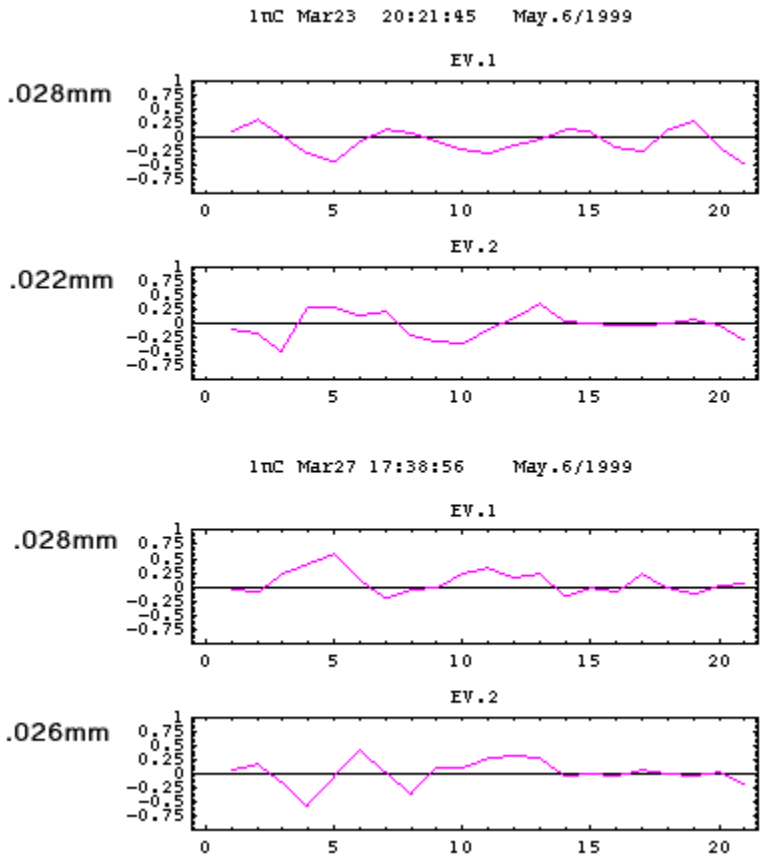


Figure 5-6: Exp: Eigenvalues and Eigenvectors

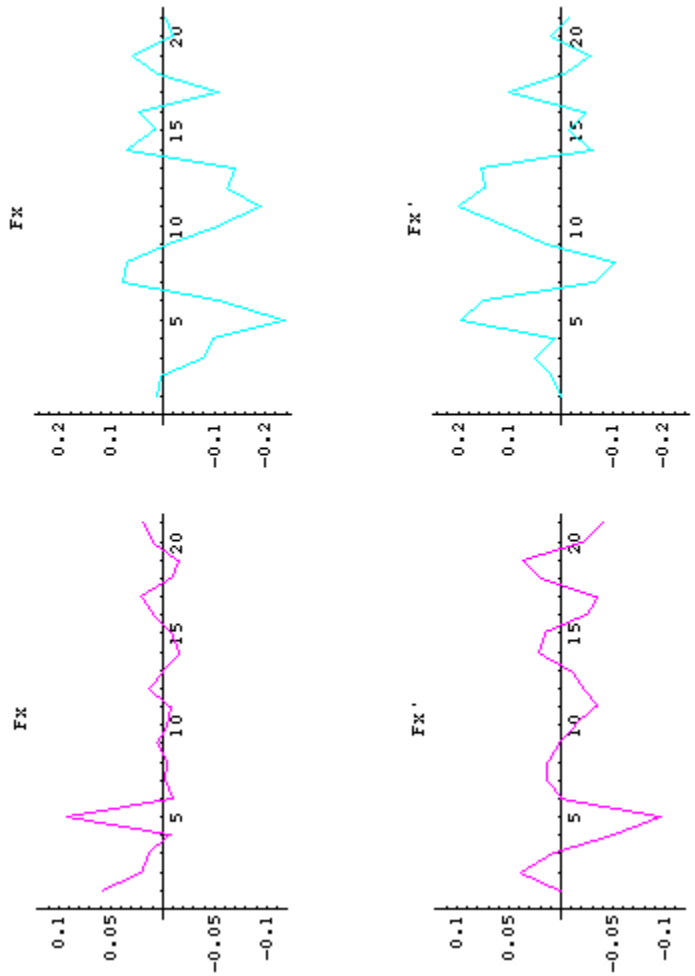


Figure 5-7: Exp: Machine model and emittance growth rate along the linac

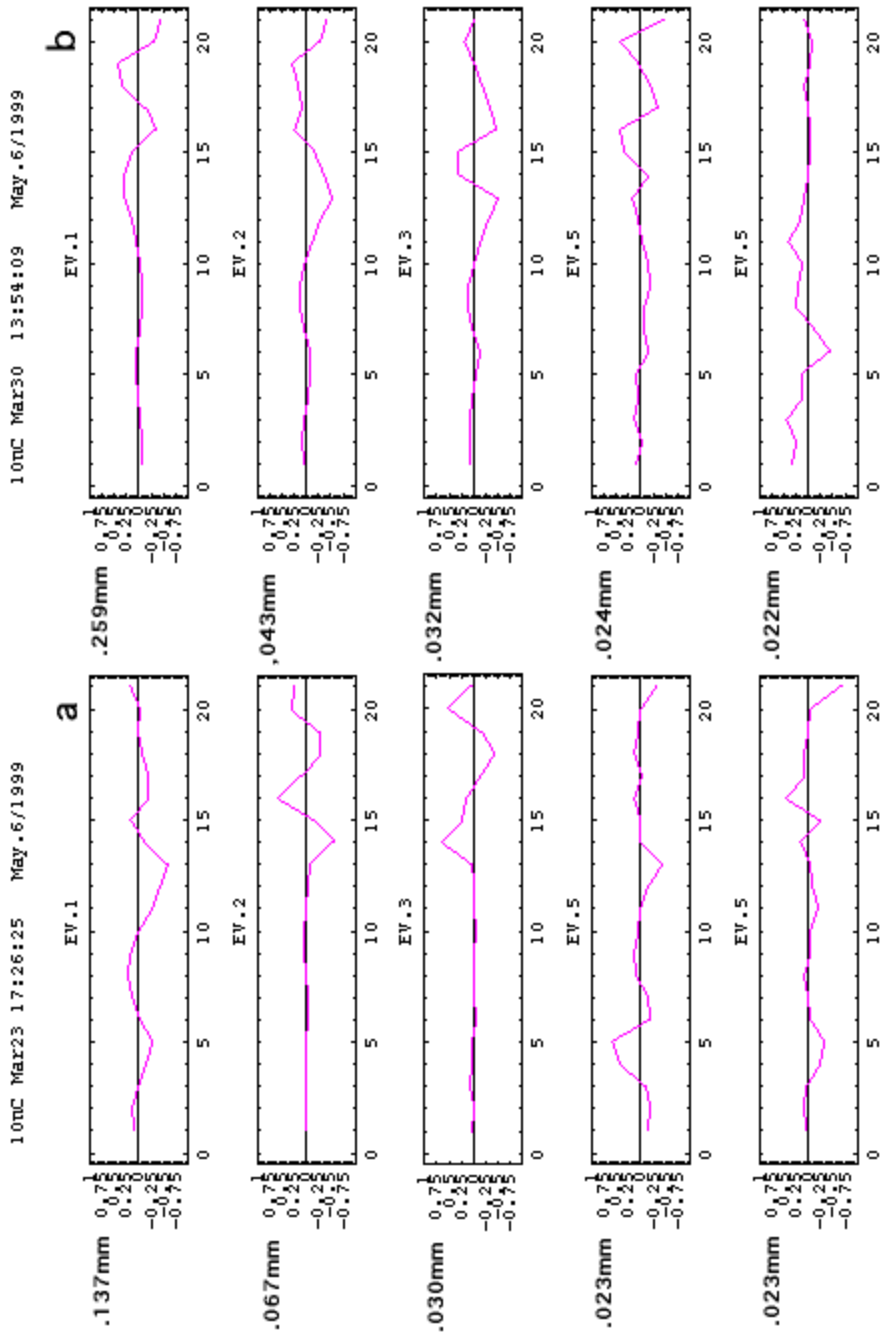


Figure 5-8: Exp: Eigenvalues and Eigenvectors

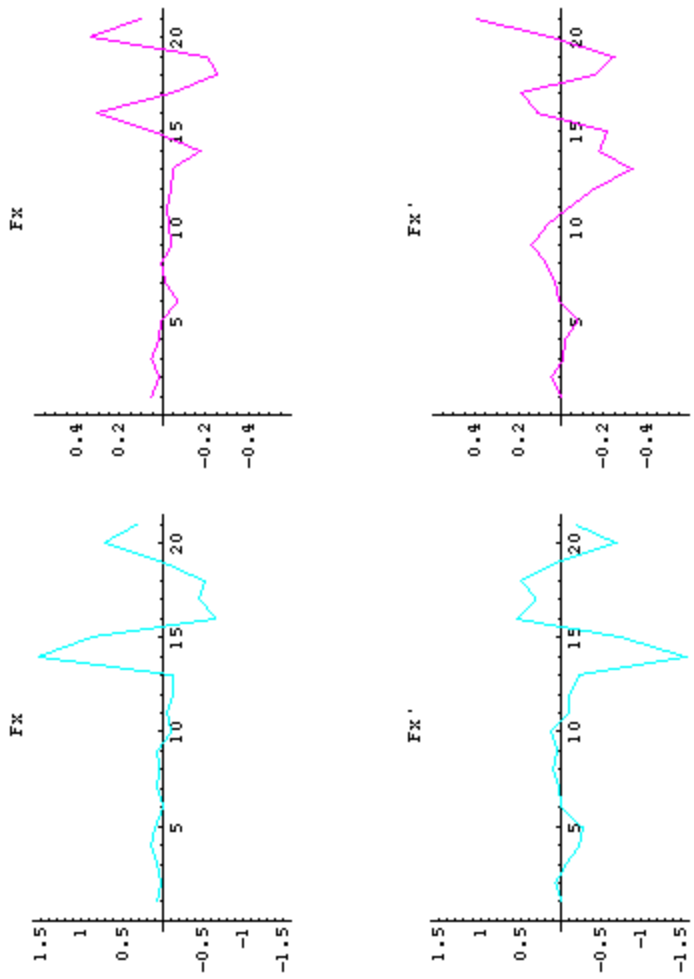


Figure 5-9: Exp: Machine model and emittance growth rate along the linac

## 5.1 Low beam current experiments

One of the most interesting results is coming out from the variance of beam orbits. Figure 5-2 shows that it is almost constant along the beam line when the linac is running in a low beam current mode. This phenomenon implies one thing: the incoming beam trajectory jitter ($x_0$ and $x\prime_0$) is quite small. Let us estimate it by the following equations:

$$\Delta x_i = n_{BPMi} + m_{11}^{0\to i}\widehat{x}_0 + m_{12}^{0\to i}\widehat{x}'_0 + \cdots \tag{5.1}$$

$$\sigma_{\Delta x}^2 = \frac{1}{P}\sum_P \left(n^2 + m_{11}^2\widehat{x}_0^2 + m_{12}^2\widehat{x}_0'^2 + 2m_{11}m_{12}\widehat{x}_0\widehat{x}'_0\right) \ . \tag{5.2}$$

The correlation coefficients between BPMs noise and injection jitters are very small, and for a large number of pulses, it is reasonable to assume them to be zero. We assume that all BPMs have the same resolution of $0.07mm$, and the injection jitter is about $\Delta x_0 = 0.04mm$ and $\Delta x'_0 = 0.04mrad$. The simulation results with machine model and experimental results are shown in Figure 5-5. Normally, the resolutions of each BPM are not the same, this transpires in Figure 5-5. So, the oscillation of the beam orbit variance comes from the injection jitter and also from the distribution of BPMs resolution. Using the experiments, we can roughly estimate that the best BPMs resolution is around 0.07mm and that the incoming beam trajectory jitters are $\Delta x_0 \leq 0.04mm$ and $\Delta x'_0 \leq 0.04mrad$.

Another interesting result is that, from the experiments, we can see that the wakefields effects are not serious at such a low beam current. This result confirms our simulation works in the previous section. The beam behavior under these conditions is more like a free betatron oscillation. The eigenvectors and the machine model are illustrated in Figure 5-6 and Figure 5-7. Because the injection jitter is so small, it is hard to separate the free betatron oscillation from BPMs noise; therefore the accuracy of our calculation of the machine model is low. In order to get a more accurate machine model, extra injection jitters ($x_0$ and $x'_0$) are needed to separate the free betatron oscilla-

tion from BPMs noise. The model obtained from experiments can be used to check our focusing scheme (the machine is almost free from the wakefields). This work, we hope, will be done in the future.

## 5.2 High beam current experiments

We are not so fortunate when beam current increases. High beam current excites very strong wakefields, which causes a much more complicated situation. In this case, the average beam orbit $b_0$ plays a very important role, but it is not easy to get a good idea of $b_0$ because of the mixing of information between the beam orbit and the BPMs offset. To obtain the BPMs offset, we need one technique called "beam based alignment" [31] which we will not discuss here. But one thing is clear, that is for different beam orbits we *do* get different E.V. plots, see Figure 5-8; it means that the machine model is affected strongly by the beam orbit, i.e., wakefields. The first eigenvector which comes from the beginning of the beam line is the betatron oscillation of the beam. A single eigenvector means that $x_0$ and $x_0'$ are correlated with each other strongly at the position of the first BPM.

Figure 5-4 and Figure 5-8 show that a big kick occured near the region of BPM#13 and BPM#14, Figure 5-2 also shows a big jump of the beam orbit variance, where Figure 5-1 shows that the average beam orbit was just normal around there. These facts tell us that a very strong wakefields kick happens there; it may come from a beam offset with respect to the axis of an accelerator structure and also from a big beta function in the vicinity, see Figure 4-1. These results also can be compared with our simulation work, and can be confirmed by another experimental result [36]. Two methods have been suggested here for solving this problem: the addition of an orbit bump and lattice re-matching. The effects of these methods have been illustrated in the simulation part. For lack of time, we have not yet done these experimentally. In a next step, we can try to change the beam orbit, rematch

the beta function along the linac, and restore the design machine model, etc. Figure 5-9 shows the machine model obtained from the experiments.

# 6 Conclusions

From the simulation study and also experimental results, we conclude that:

1. The accuracy of BPMs measurements can be improved by $\sqrt{D \ / \ M}$ .
2. The real machine model can be obtained from BPM reading matrix.
3. The places of variable sources which cause beam orbits fluctuation can be located.
4. The wakefield effects can be observed.

# 7 Future prospect

Because of the lack of time, most of the work presented here is based on incomplete simulations. We need to do more experiments in the future to perfect our simulation work.

First we hope to use more time patterns to get more a detailed machine model. In order to get the free betatron machine model, we need to add some initial jitters at the beginning of the beam line.

The second thing we want to do in the future is to study the effect of BNS damping. From [36] we know that when the KEKB injector linac is running in a high current mode, the beam emittance dilution rate is about 8. It is a quite large number; from the simulation we see that by adjusting the accelerating phase, some amount of correlated energy spread can be introduced into the bunch and make the emittance dilution rate small.

Finally, we can try lattice re-matching and orbit steering to alleviate the emittance dilution.

Also the experiments may reveal more pitfalls than the simulation. The method can end up being more complicated than expected.

# 8 Acknowledgment

First I would like to express my sincere gratitude to Prof. S. Kurokawa for offering me the opportunity to study here and for his continuous support.

I want to thank in particular Prof. E. Forest for all his help. I have benefited a lot from discussing with him and learning from him. I admire his attitude towards the science.

Prof. Koiso helped me a lot with the program SAD and experimental things, etc. I have also learned a lot from discussing with her.

I had some useful discussions with Prof. Kamada and Prof. Yokoya. Prof. Yokoya gave me his new formulas for the calculation of wakefields.

Finally, I want to express my special thanks to Profs. J. Irwin, Y. Yan, K. Bane and Dr. C.X. Wang. I learned MIA from them, also they gave me many good advises on my work. I thank Prof. Irwin for his hospitality during my short visit to SLAC.

# 9 Appendix

The time pattern and SVD methods are based on measurememnts of the average beam position. Unfortunately in the presence of strong collective effects it is not possible to compute the emittance of the full beam on the basis of these measurements alone. In the presence of wake fields we can hope to correlate the growth in emittance with an MIA analysis, but, it requires a model or additional measurements.

A collective effect can blow or shrink a distribution while not affecting at all the motion of the average of the distribution. For example, electrons traveling side by side along the "$z$" direction will slowly move apart due to the electro-static repulsion. If we imagine these electrons uniformly distributed around $(x, x') = (0, 0)$ they will remain centered around $(x, x') = (0, 0)$ after a free propagation. However the emittance will have grown due to the repulsive interaction. Indeed centered electron will have developed a radial motion i.e., $x' \neq 0$. This situation is obviously the worse possible scenario. In the case of wake fields, the average transport matrix (which we will denote by $\Gamma$ in this appendix) affects the average beam position, the emittance and is correlated to the real emittance. The only problem is that we do not know the true relationship without a model or additional measurements.

This is to be contrasted with a single particle effect such as acceleration or classical radiation. These processes affect each particle individually in an nearly identical manner. Therefore, in the linear regime where filamentation is absent, the motion of the average beam will faithfully represent the motion of each individual particle. In this case we can hope to obtain the emittance dilution on the basis of an average BPM measurements alone in a virtually perfect Model Independent setting.

## 9.1 Theoretical Analysis

To see how things get more complicated in the collective case, let us computed the emittance in the presence of wake fields by postulationg the existence of some linear operators.

At the entrance of the linac, we divided the beam longitunally in $N = 100$ macro particles. We will assume that each macro particle (or pancake) has some structure, therefore the initial coordinates of an actual particle in the $j^{th}$ pancake are given by

$$\vec{x}^j(0) = \vec{Y}^j(0) + \vec{\xi}^j(0). \tag{9.1}$$

The average of the internal pancake variable $\vec{\xi}$ are zero by definition. The first pancake is denoted by $j = 1$ and the last pancake by $j = N = 100$.

Down the lattice, at a position $s$, we can again express the state of the beam in a similar manner:

$$\vec{x}^j(s) = \vec{Y}^j(s) + \vec{\xi}^j(s) \text{ with } \left\langle \vec{x}^j \right\rangle = \vec{Y}^j. \tag{9.2}$$

To understand how the collective effects enter in the definition of the emittance, we need to postulate a form for the operator from $s = 0$ to $s$:

$$\vec{x}^j(s) = M\vec{\xi}^j(0) + \sum_{i=1}^{N=100} T^{j\,i}\vec{Y}^i(0). \tag{9.3}$$

Actually in Eq. (9.3), the sum over the pancakes can be carried from $i = 1$ to $j$ because of the nature of the wake field. However, it is not an important feature. The matrice $T^{j\,i}$ connect the phase space of the $i^{\text{th}}$ to the $j^{\text{th}}$; there are a lot of these matrices and they include the collective effect. The matrix $M$ is the matrix of the beam line in the absence of collective effects (zero current). Eq. (9.3) can be derived by looking at the collective kick between $s$ and $s + ds$: eventhough the wake field kick acts on all the coordinates of the trailing pancakes, because it is a dipole kick, it will only affect $\vec{Y}^j(s)$ and

not $\vec{\xi}^j(s)$. If we re-expressed $\vec{x}^j(s)$ in terms of the average over the pancake, we get:

$$\begin{aligned}
\vec{Y}^j(s) &= \sum_{i=1}^{N=100} T^{j\,i}\vec{Y}^i(0), \\
\vec{\xi}^j(s) &= M\vec{\xi}^j(0), \\
\text{with } \vec{x}^j(s) &= \vec{Y}^j(s) + \vec{\xi}^j(s)
\end{aligned} \tag{9.4}$$

To proceed further, we split the matrices $T^{j\,i}$ into a single particle dynamics part and a collective part:

$$T^{j\,i} = M + \ C^{j\,i}, \tag{9.5}$$

where the matrix $C^{j\,i}$ depends on the current $i_c$.

We substitute this expression into Eq. (9.4).

$$\vec{Y}^j(s) = M\vec{Y}^j(0) + \sum_{i=1}^{N=100} C^{j\,i}\vec{Y}^i(0) \tag{9.6}$$

In our simulations the average pancake starting positions and momenta were all the same. Therefore we can simplify Eq. (9.6) into[3]

$$\begin{aligned}
\vec{Y}^j(s) &= \left\{ M + \sum_{i=1}^{N=100} C^{j\,i} \right\} \ \vec{Y}(0) \\
&= \left\{ M + G^j \right\} \vec{Y}(0).
\end{aligned} \tag{9.7}$$

We are now ready to perform the averages which enter in the theory as well as the experiments. These averages must be over the pancakes as well as over the internal structure of the pancakes (over $\xi$). We start with the average

[3]The particle coordinates are at $s = 0$ which is different from $t = 0$. However this is a tiny correction at the entrance of the linac as pancakes would have to drift forwards or backwards in order to collapse to the plane $s = 0$. The end result is a slightly different collective matrix.

of the position and momentum which are quantities directly extracted from the BPM measurements:

$$\langle x_a \rangle_s = \sum_\alpha \left\{ M_{a\alpha} + \underbrace{\frac{1}{N} \sum_{j=1}^{N=100} G^j_{a\alpha}}_{\Gamma_{a\alpha}} \right\} Y_\alpha(0) = \sum_\alpha \left\{ M_{a\alpha} + \Gamma_{a\alpha} \right\} Y_\alpha(0). \quad (9.8)$$

The matrix $\Gamma$ in Eq. (9.8) defines the average effects of the collective kick at position $s$. As explained before, it could vanish in theory. However it is definitely non-zero for the tranverse wake field effect as shown by the experiments and the simulation. The next step is to compute the average of the quadratic moments at $s$:

$$\langle x_a x_b \rangle_s = \sum_{\alpha,\beta} \left\{ \left\{ M_{a\alpha} M_{b\beta} + \frac{1}{N} \sum_{j=1}^{N=100} G^j_{a\alpha} G^j_{b\beta} + M_{a\alpha} \Gamma_{b\beta} + M_{b\beta} \Gamma_{a\alpha} \right\} Y_\alpha(0) Y_\beta(0) + M_{a\alpha} M_{b\beta} \langle \xi_\alpha \xi_\beta \rangle \right\}. \quad (9.9)$$

The average of Eq. (9.8) is clearly measureable from the BPM data. Therefore we need to compare the square of the BPM measurements (Eq. (9.8)) with the averages given by Eq. (9.9).

$$\begin{aligned} \Sigma_{ab} = \langle x_a x_b \rangle_s - \langle x_a \rangle_s \langle x_b \rangle_s &= \sum_{\alpha,\beta} \left\{ \frac{1}{N} \sum_{j=1}^{N=100} G^j_{a\alpha} G^j_{b\beta} - \Gamma_{a\alpha} \Gamma_{b\beta} \right\} Y_\alpha(0) Y_\beta(0) \\ &\quad + \sum_{\alpha,\beta} M_{a\alpha} M_{b\beta} \langle \xi_\alpha \xi_\beta \rangle \\ &= \sum_{\alpha,\beta} \left\{ \Sigma^{ab}_{\alpha\beta} Y_\alpha(0) Y_\beta(0) + M_{a\alpha} M_{b\beta} \langle \xi_\alpha \xi_\beta \rangle \right\}. \quad (9.10) \end{aligned}$$

The emittance of the beam is then obtained from Eq. (9.10)

$$\varepsilon = \sqrt{\Sigma_{11}\Sigma_{22} - \Sigma_{12}^2}. \quad (9.11)$$

In Eq. (9.10) we see that the difference between the BPM measurements and the averages is given by a quadratic form that is the variance of the matrices $G^j$ over the pancakes. This quantity cannot obtained with the standard MIA without using some model.

In addition there is a term which depends on the internal structure of each pancake and the single particle matrix (or zero current matrix). If the initial distribution sits on an ellipse described by some Twiss parameters $\alpha$, $\beta$, and $\gamma$, then Eq. (9.10) can be rewritten in terms of the initial emittance of the internal variables

$$\varepsilon_0 = \sqrt{\langle \xi_1^2 \rangle \langle \xi_2^2 \rangle - \left\langle \xi_1 \xi_2 \right\rangle^2},$$

the determant of the matrix $M$ which turns out to be the ratio of the exit over the entrance relativistic gamma factor, and in terms of the propagated Twiss parameters of the distribution. For example, the beam size in $x$ reduces to:

$$\sum_{\alpha,\beta} M_{1\alpha} M_{1\beta} \left\langle \xi_1^2 \right\rangle = \frac{\gamma(s)}{\gamma(0)} \beta(s) \varepsilon_0. \tag{9.12}$$

There is one other quantity of physical interest, which can be computed with the BPM measurement directly. It is the spread of the measured $x$ and deduced $x'$ over the pulses. This quantity is related directly to the matrix $\Gamma$. Let us called it the "barycentre emittance" and denote it $\varepsilon_P$. To compute it we need compute the variance over the pulses:

$$\begin{aligned} \langle \langle x_a \rangle \langle x_b \rangle \rangle_P &= \frac{1}{P} \sum_{p=1}^{P} \langle x_a \rangle_{s;p} \langle x_b \rangle_{s;p} - \underbrace{\langle \langle x_a \rangle \rangle_P \langle \langle x_b \rangle \rangle_P}_{=0 \text{ by construction}} \\ &= \sum_{p=1}^{P} \left\{ \sum_{\alpha,\beta}^{\infty} \{M_{a\alpha} + \Gamma_{a\alpha}\} \{M_{b\beta} + \Gamma_{b\beta}\} \right\} Y_{\alpha;p}(0) Y_{\beta;p}(0). \end{aligned} \tag{9.13}$$

We can also add to this quantity the pancake emittances due to initial spread

in each pancake as we did in Eq. (9.10):

$$\Sigma_{ab}^{P} = \langle \langle x_a \rangle \langle x_b \rangle \rangle_P - \sum_{\alpha,\beta} M_{a\alpha} M_{b\beta} \langle \xi_\alpha \xi_\beta \rangle \,. \tag{9.14}$$

The barycentre emittance is then given by

$$\varepsilon_P = \sqrt{\Sigma_{11}^{P} \Sigma_{22}^{P} - \Sigma_{12}^{P\,2}}. \tag{9.15}$$

This barycentre emittance that represent the scattering of the pulses barycentres and is computable from measured data alone. Unfortunately it does not given the full picture of our beam.

## 9.2 Experimental and Numerical Results

The best we can do under the present circumstances is to estimate the range of the true emittance of Eq. (9.15) with our measured data and the model used in this thesis for the wakefield effects.

We will use the data corresponding to Figure 5-8, experiment **b**. In this experiment the current was 10 nC. We will use the measured data at the BPM # 20 as well as the deduced value of $x'$. These are plotted on Figure 9-1. The values on this plot are well above the noise floor which is approximately at 0.1mm. The initial distribution near the entrance cannot be measured with the same relative accuracy simply because it still sits "within" the noise floor. We simply did not have enough pulses or/and sufficiently accurate BPMs.

First we choose two initial conditions for the center of the incoming distribution. Calling this initial ray $\vec{x}^{off}$ the "offset," we first selected no offset,i.e., $\vec{x}^{off} = (0, 0)$. The second offset selected was $\vec{x}^{off} = (30\mu, 0)$ because it is large but still physically sensible. It will give us an idea of the possible emittance growth due to a misaligned structure.

We then tracked the 100 pancakes forward until the $20^{\text{th}}$ BPM. A map was computed as a Taylor series relating the final averages $\vec{Y}(s)$ to the initial

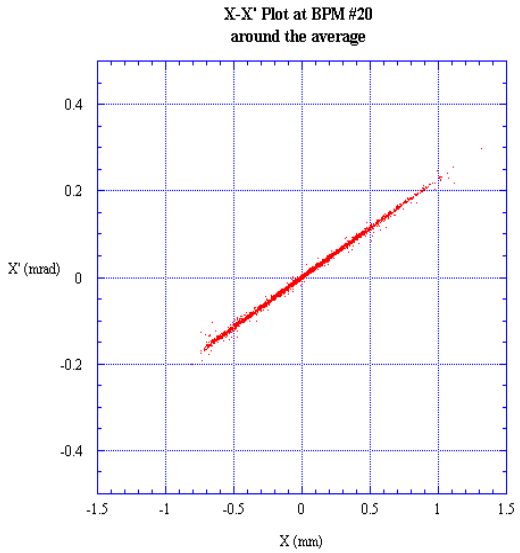


Figure 9-1: Exp: Final Data at BPM # 20 expressed around the average.

displacements of the pancakes $\vec{Y}(0)$. This map is, in the linear approximation, the matrix $M + \Gamma$ of Eq. (9.8).

Therefore our first calculation consist in tracking these particles backwards to the initial plane $s = 0$. We perform this calculation by using the inverse of the approximate map expressing the final rays and average beam sizes as a function of the initial values.

We then tracked this distribution with and without the offset. We computed the ratio of the emittance with collective effects over the emittance without collective effects.

We found that the ideal lattice with no injection errors produces an emittance growth of only 2.2. The second calculation, done with an offset of 30 microns, gave an emittance growth of 5.9. The emittance of some pulses actually grew by as much as 14.7.

To proceed further we would need to model the experiment more closely by introducing some misaligned structures and the closed orbit corrections

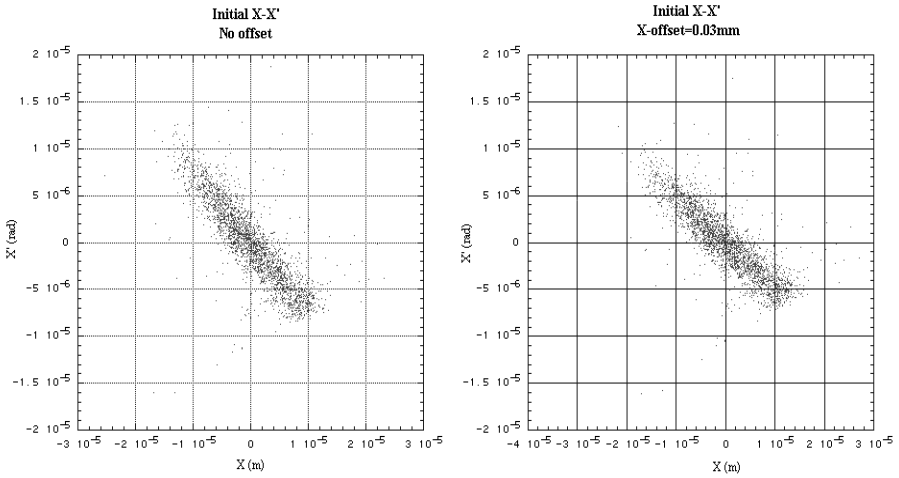


Figure 9-2: Exp: Final Data at BPM # 20 expressed around the average.

used in the experiments. This requires a lot more work.

# References


[1] J. Irwin, C.X. Wang, Y.T. Yan, K. Bane, Y. Cai, F. Decker, M. Minty, G. Stupakov, F. Zimmermann, "Model-Independent Analysis with BPM Correlation Matrices," SLAC-PUB-7863, June 1998.

[2] J. Irwin, C.X. Wang, K. Bane, Y.T. Yan, M. Minty, F. Decker, G. Stupakov, "Transverse Wakefield Effect Measurement via Model-Independent Analysis," SLAC-PUB-7917, August 1998.

[3] Private communication with J. Irwin.

[4] Private communication with C.X. Wang.

[5] Private communication with Y.T. Yan.

[6] KEKB B-Factory Design Report, KEK Report 95-7, August 1995(A).

[7] KEK Report 95-18, March 1996(A).

[8] JLC Design Study, KEK Report 97-1, April 1997.

[9] J. Rees, "The Principles and Construction of Linear Colliders," SLAC-PUB-4073, September 1986(E/A).

[10] R. Assmann and F. Zimmermann, "Possible Sources of Pulse-To-Pulse Orbit Variation in the SLAC Linac," SLAC-PUB-7269, August 1996.

[11] J.T. Seeman, "Beam Dynamics Issues in Linear Colliders," SLAC-PUB-4886, June 1989(A).

[12] V.M. Tsakanov, "Emittance Dillution of the Correlated Energy Spread, Single Bunch Instability and Lattice Scaling in LC," DESY M 96-02, February 1996.

[13] J.T. Seeman, "SLC Beam Dynamics Issues," SLAC-PUB-5717, December 1991(A).

[14] Ralph W. Assmann, "Beam Dynamics in SLC," SLAC-PUB-7576, July 1997.

[15] T.O. Raubenheimer, Ph.D. thesis, SLAC-387, UC-414(A).

[16] Mathematica (Stephen Wolfram, Redwood City, 1991).

[17] SAD manual.

[18] MAD manual.

[19] Transport manual.

[20] V.E. Balakin, A.V. Novokhatsky and V.P. Smirnov, "VLEPP: TRANSVERSE BEAM DYNAMICS," Proc. of the 12th Inter. Conf. on High Energy Accelerator. P119-120.

[21] V.M. Tsakanov, "Autophasing and lattice scaling in high energy linear accelerators," Physical Review Special Topics - Accelerators and Beams, Vol.1(1998).

[22] TBCI manual.

[23] ABCI manual.

[24] T.O. Raubenheimer and K. Kubo, "A technique of measuring and correcting emittance dilutions due to accelerator structure misalignments," NIM A370(1986) 303-311.

[25] W.L. Spence, "BNS damping - 'Autophasing' and discrete Focusing," International Workshop on Emittance Preservation in Linear Colliders, KEK/Tsukuba/Japan 19-23 April 1993.

[26] G.V. Stupakov, "BNS Damping of Beam Breakup Instability," SLAC-AP 108, August 1997.

[27] F.J. Decker, et. al., "Dispersion and Betatron Matching into the Linac," Proc. of the 1991 Part. Acc. Conf., San Francisco, CA (1991); and SLAC-PUB-5484.

[28] N. Merminga, P.L. Morton, J.T. Seeman, W.L. Spence, "Transverse Phase Space in the Presence of Dispersion," Proc. of 1991 Part. Acc. Conf., San Francisco, CA (1991); and SLAC-PUB-5514.

[29] T.O. Raubenheimer and R.D. Ruth, "A Dispersion-Free Trajectory Correction Technique for Linear Colliders," Nucl. Instr. Meth., A302 191 (1991).

[30] Numerical Recipes.

[31] C.E. Adolphsen, "Beam-Based Alignment Technique for the SLC Linac," SLAC-PUB-4902/LBL-27057, March 1989(A).

[32] J.T. Seeman, "Observation and Cures of Wakefield Effects in the SLC Linac," SLAC-PUB-5716, December 1991(A).

[33] T. Limberg, J.T. Seeman and W.L. Spence, "Effects and Tolerances of Injection Jitter in the SLC and Future Linear Colliders," SLAC-PUB-5276, May 1990(A).

[34] J.T. Semman and F.-J. Decker, "The Introduction of Trajectory Oscillations to Reduce Emittance Growth in The SLC Linac," SLAC-PUB-5705, August 1992(A).

[35] Private communication with K. Yokoya.

[36] T. Kamitani, H. Koiso, et al. "Beam Optics Matching in the KEKB Injector Linac," KEK Preprint 98-91, July 1998(A).

[37] A.W. Chao, B. Richter, and C.Y. Yao, "Beam Emittance Growth Caused by Transverse Deflecting Fields in a Linear Accelerator," NIM 178(1980) 1-8.

[38] A.W. Chao, Physics of Collective Beam Instabilities in High Energy Accelerators (Wiley, New York, 1993).

[39] C.X. Wang, Ph.D. thesis, unpublished yet.